Universidade
Estadual de Londrina

HEITOR CASASOLA

FRACTAL SUBSYSTEM SYMMETRIES, UV/IR MIXING, AND ANOMALIES

Londrina
2024

Heitor Casasola

Fractal Subsystem Symmetries, UV/IR Mixing, and Anomalies

Trabalho apresentado ao Departamento de Física da Universidade Estadual de Londrina, como requisito parcial à obtenção do título de Doutor.

Universidade Estadual de Londrina
Departamento de Física
Programa de Pós-Graduação em Física

Orientadora: Dra. Paula Fernanda Bienzobas

Londrina
03 de Maio de 2024

Ficha de identificação da obra elaborada pelo autor, através do Programa de Geração Automática do Sistema de Bibliotecas da UEL

H473f Casasola, Heitor
Fractal Subsystem Symmetries, UV/IR Mixing, and Anomalies / Heitor Casasola. – Londrina, 2024.
46f. : il.

Orientadora: Dra. Paula Fernanda Bienzobas
Tese (Doutorado em Física) – Universidade Estadual de Londrina, Centro de Ciências Exatas, Programa de Pós-Graduação em Física, 2024.
Inclui bibliografia.

1. Strong correlated electrons – Tese. 2. Fractal Subsystem Symmetries – Tese. 3. Topologically ordered phases of matter – Tese. I. Bienzobas, Paula Fernanda. II. Universidade Estadual de Londrina. Centro de Ciências Exatas. Programa de Pós-Graduação em Física. III. Título.

CDU 53

Heitor Casasola

Fractal Subsystem Symmetries, UV/IR Mixing, and Anomalies

Trabalho apresentado ao Departamento de Física da Universidade Estadual de Londrina, como requisito parcial à obtenção do título de Doutor.

BANCA EXAMINADORA

Orientadora: Dra. Paula Fernanda Bienzobas
Universidade Estadual de Londrina

Dr. Carlos André Hernaski
Universidade Estadual de Londrina

Dr. Rodrigo Goncalves Pereira
Universidade Federal do Rio Grande do Norte

Dr. Carlos Eduardo Fiore dos Santos
Universidade de São Paulo

Dr. Weslei Bernardino Fontana
National Tsing Hua University

Dr. Pedro Rogerio Sergi Gomes
Universidade Estadual de Londrina

Dr. Rodrigo Corso B. Santos
Universidade Estadual de Londrina

Londrina, 03 de Maio de 2024

Dedico este trabalho a Deus e a Maria por me capacitarem e me guiarem ao longo desta jornada acadêmica.

Também dedico este trabalho a toda a minha família, cujo apoio incondicional foi fundamental em cada etapa do meu doutorado. Em especial, expresso minha profunda gratidão à minha mãe, cujos sacrifícios e incentivos foram uma fonte constante de inspiração.

À minha amada esposa Érica, que é minha parceira desde os primeiros dias na graduação. Sua paciência infinita ao ouvir minhas explicações sobre todo tipo de assunto, mesmo quando pareciam desconexos, é um verdadeiro exemplo de amor e apoio inabaláveis. Agradeço por estar sempre ao meu lado, nutrindo-me com amor, cuidado, carinho, apoio e compreensão.

Agradecimentos

Gostaria de expressar minha profunda gratidão a todos os meus colegas físicos e amigos, cujas discussões e debates contribuíram significativamente para o meu crescimento como pesquisador. Em particular, quero agradecer ao Julio pelas discussões que tivemos.

Um agradecimento especial ao meu amigo Guilherme pela sua valiosa participação nesta pesquisa, compartilhando seu conhecimento e oferecendo suporte durante o período de intercâmbio. Sua colaboração foi fundamental para o desenvolvimento desta pesquisa.

Durante meu doutorado, tive a oportunidade enriquecedora de visitar a Boston University como aluno pesquisador. Gostaria de agradecer ao Professor Claudio Chamon por ter aceitado me receber em seu grupo de pesquisa. Agradeço imensamente a Mirtha Cabello pelo seu acolhimento caloroso que tornou possível a minha estadia em Boston.

Expresso minha gratidão aos membros da banca examinadora por aceitarem o convite e por suas contribuições valiosas, correções e questões levantadas, que enriqueceram profundamente este trabalho.

Quero estender meus agradecimentos ao Prof. Pedro R. S. Gomes, que tem sido um mentor desde os dias de graduação, proporcionando orientação, discussões enriquecedoras e ensinamentos valiosos que moldaram meu desenvolvimento acadêmico e pessoal.

Por fim, gostaria de dedicar um agradecimento especial à minha orientadora e amiga, Profa. Paula Bienzobas, pela dedicação, orientação e apoio incansáveis nas mais diversas situações ao longo deste percurso. Suas discussões estimulantes e ensinamentos sobre física foram fundamentais para minha formação como pesquisador. Além disso, acredito sinceramente que saio deste doutorado como um ser humano um pouquinho melhor, graças a tudo que aprendi com ela.

O presente trabalho foi realizado com o apoio da Coordenação de Aperfeiçoamento de Pessoal de Nível Superior - Brasil (CAPES) e do Conselho Nacional de Desenvolvimento Científico e Tecnológico (CNPq).

"Nosso grande adversário está dentro de cada um de nós... Devemos procurar ser melhor hoje do que aquilo que fomos ontem."

Abel Ferreira

Resumo

Neste trabalho, estudamos fases topologicamente ordenadas anisotrópicas e não convencionais em $3d$ que manifestam a física fractônica do tipo II ao longo de *submanifolds*. Enquanto se comportam como uma ordem topológica usual ao longo de uma direção espacial preferencial, sua física ao longo de planos perpendiculares é ditada pela presença de simetrias de subsistemas fractais, restringindo completamente a mobilidade das excitações anyônicas e seus estados ligados. Consideramos uma realização explícita de modelo de rede para tais fases e estudamos suas propriedades sob condições de contorno periódicas e, posteriormente, na presença de bordas. Além disso, generalizamos nosso estudo para sistemas fractais com tamanhos $L_x \neq L_y$. Descobrimos que para tamanhos específicos de rede, o sistema possui simetrias de linha e de membrana fractais que são mutuamente anômalas, resultando em um estado fundamental com gap de energia não trivial. Isso corresponde à quebra espontânea das simetrias fractais, implicando em uma degenerescência subextensiva do estado fundamental. Para os tamanhos restantes, as simetrias fractais são explicitamente quebradas pelas condições de contorno periódicas, o que está intrinsecamente relacionado à unicidade do estado fundamental. Apesar disso, o sistema ainda é topologicamente ordenado, uma vez que as quase-partículas criadas localmente têm estatísticas mútua não triviais e, na presença de bordas, ainda apresenta modos de borda anômalos. A forte dependência de simetrias pelo tamanho da rede é uma manifestação ímpar da mistura ultravioleta/infravermelha (UV/IR). Também elucidamos a física dessas fases em uma variedade com bordas e discutimos o *anomaly inflow*. Ao nos concentrarmos exclusivamente na física de borda, estabelecemos uma conexão entre esta fase e uma fase topológica protegida por simetria ou uma fase de quebra espontânea de simetria. Usando a teoria efetiva, demonstramos que simetrias mutuamente anômalas na borda não podem ser simultaneamente quebradas.

Palavras-chave: 1. Elétrons Fortemente Correlacionados 2. Física de Alta Energia - Teoria 3. Simetrias de Subsistema Fractal.

Casasola, Heitor. **Fractal Subsystem Symmetries, UV/IR Mixing, and Anomalies**. 2024. Tese de Doutorado em Física – Universidade Estadual de Londrina, Londrina, 2024.

Abstract

In this work, we study unconventional anisotropic topologically ordered phases in $3d$ that manifest type-II fractonic physics along submanifolds. While they behave as usual topological order along a preferred spatial direction, their physics along perpendicular planes is dictated by the presence of fractal subsystem symmetries, completely restricting the mobility of anyonic excitations and their bound states. We consider an explicit lattice model realization of such phases and proceed to study their properties under periodic boundary conditions and, later, in the presence of boundaries. Furthermore, we generalize our study to fractal systems with unequal sizes $L_x \neq L_y$. We find that for specific lattice sizes, the system possesses line and fractal membrane symmetries that are mutually anomalous, resulting in a nontrivially gapped ground state space. This amounts to the spontaneous breaking of the fractal symmetries, implying a subextensive ground state degeneracy. For the remaining system sizes the fractal symmetries are explicitly broken by the periodic boundary conditions, which is intrinsically related to the uniqueness of the ground state. Despite that, the system is still topologically ordered since locally created quasiparticles have nontrivial mutual statistics and, in the presence of boundaries, it still presents anomalous edge modes. The intricate symmetry interplay dictated by the lattice size is a wild manifestation of ultraviolet/infrared (UV/IR) mixing. We also elucidate the physics of these phases in a manifold with boundaries and discussed the anomaly inflow. By focusing solely on boundary physics, we establish a connection between this phase and either a Symmetry Protected Topological phase or a Spontaneous Symmetry Breaking phase. Using effective theory, we demonstrate that mutually anomalous symmetries at the boundary cannot be simultaneously broken.

Keywords: 1. Strongly Correlated Electrons 2. High Energy Physics - Theory 3. Fractal Subsystem Symmetries .

Casasola, Heitor. **Fractal Subsystem Symmetries, UV/IR Mixing, and Anomalies**. 2024. Ph. D. in Physics Thesis – Universidade Estadual de Londrina, Londrina, 2024.

List of Figures

Figure 1 – In the left a representation of hexagonal close-packed lattice and in the right a TD operator. . . . 3
Figure 2 – In (a) the TD operators has two sites in common, whereas in (b) and (c) they share a single site. . . . 4
Figure 3 – The xy-plane. . . . 5
Figure 4 – In Figure (a) the t_{p_j} are represented in the original triangular lattice, and in Figure (b) the positions new notation of $t_{j,i}$. . . . 6
Figure 5 – Example of a configuration generated by Eq. (2.20) in a lattice of size 6×6 . . . 7
Figure 6 – For $L_y = 5$ and $L_x = 15$, defining $\bar{S}_1^1(x) = S_1^1(x) + S_6^1(x) + S_{11}^1(x)$, the first line respects $\bar{S}_1^1(x) = \bar{S}_6^1(x)$. On the left it shows $S_1^1(x)$, $S_6^1(x)$, and $S_{11}^1(x)$, and on the right is depicted a 15×5 configuration (the first and de last rows are the same). . . . 8
Figure 7 – The product of TD operators along the z-direction, reducing to the product of three Wilson lines. . . . 12
Figure 8 – The membranes generated by $S_1^i(x)$ and $\tilde{S}_1^i(x)$, where $i = 1, 2, \ldots, 6$, in system of size $L = 7$. Each membrane highlights the unique $t_{ij} = 1$ that do not repeat in other membranes. . . . 14
Figure 9 – For non-degenerated system sizes, a single X_k operator can be obtained by the product of TD operators over a plane. The figures above depict this product for $L = 4$, $L = 5$, and $L = 10$. . . . 16
Figure 10 – Sequence of movements reflecting mutual statistics among excitations. 18
Figure 11 – Local splitability of the Wilson line. . . . 20
Figure 12 – An top boundary of lattice open in z-direction and the representation of P_j^b and Q_j^b operators. . . . 21
Figure 13 – Representation of $\tilde{P}_j^t$ and $\tilde{Q}_j^t$ operators. They are constructed as products of P_j^t and Q_j^t, respectively, with TD operators. . . . 22
Figure 14 – Representations of $\tilde{P}$ and $\tilde{Q}$ in the bulk. In the first figure, both operators $\tilde{P}$ and $\tilde{Q}$ are attached in the top boundary and the anomaly in the bulk is highlighted. In the last two figures, one operator is attached in the top boundary while the other originates from the bottom boundary, resulting in them not being mutually anomalous. . . . 22
Figure 15 – Representation of different choices of α and β for different lattice structures. The Wilson lines are represented in red only in the cases that the choices allows this symmetry. . . . 25

Figure 16 – The resulting systems in ≈ 2d. In the cases V to $VIII$ we verify that $\mathcal{O}$ is still fitting in the lattice. 25
Figure 17 – The membranes generated by $S_1^i(x)$, where $i = 1, 2, \ldots, 6$, respectively, in system of size $L = 7$. 44
Figure 18 – The first three configurations are generated by the Eq. (A.3) and the last one by Eq. (A.4). The configurations are depicted with eight rows and seven columns, the extra row included in the end is equivalent to the first one by periodic boundary conditions. We can check that while the first three configurations are periodic in a size 7×7, the last one to not respects the periodicity. 44
Figure 19 – The membranes generated by $S_1^i(x)$, where $i = 1$, 2, 3, and 4, respectively, in system of size $L = 6$. 45
Figure 20 – The first and second configurations are generated by Eq. (A.7) and the last one is generated by Eq.(A.8). The configurations are depicted with seven rows and six columns, the extra row included in the end is equivalent to the first one by periodic boundary conditions. We can check that while the first two configurations are periodic in a size 6×6, the last one to not respects the periodicity. 45
Figure 21 – Periodic configurations for 3×3, 6×6, and 9×9 respectively. 46

Contents

1 INTRODUCTION 1

2 TOPOLOGICALLY ORDERED FRACTAL PHASE 3
2.1 Ground State Degeneracy 4
2.2 Sizes with $L_x = L_y = L$ 4
2.3 Sizes with $L_x \neq L_y$ 7

3 SYMMETRY OPERATORS AND MIXED 'T HOOFT ANOMALIES 11
3.1 Wilson Lines 11
3.2 Fractal Membranes 12
3.3 Mixed 't Hooft Anomaly 13

4 NON-DEGENERATE CASES 15

5 EXCITATIONS AND MUTUAL STATISTICS 17

6 SPONTANEOUS BREAKING OF SUBSYSTEM SYMMETRIES 19

7 BOUNDARY THEORY 21
7.1 Anomaly Inflow 21
7.1.1 Anomaly Inflow in Non-Degenerated System Sizes 23
7.1.2 Anomaly Inflow in Degenerated System Sizes 23
7.2 Connection with Fractal 2d models 23

8 EFFECTIVE FIELD THEORY AND EDGE MODES 27

9 CONCLUSIONS 33

REFERENCES 35

APPENDIX 41

A FRACTAL CONFIGURATIONS 43

1 Introduction

It is quite remarkable that certain elementary systems, containing simple degrees of freedom that interact only locally, can give rise to exotic forms of matter [1]. Topologically ordered systems are among the most prominent examples, with emergent quasiparticle excitations carrying anyonic statistics. Fractonic topological ordered systems are even more exotic [2–15], with excitations that are intrinsically devoid of mobility due to the existence of generalized forms of symmetries known as *subsystem* symmetries [16–19].

Subsystem symmetries are generated by conserved charges along rigid spatial subdimensional manifolds, which tend to be extremely sensible to the underlying lattice geometry. Compliance with such conservation laws imposes severe restrictions on the mobility of the excitations. This contrasts with usual topological order, which is in general characterized by topologically deformable symmetry generators, known as *higher-form* symmetries, and poses no constrains on excitation's mobility [20–24].

Abelian topological order and fractonic phases may be rephrased in terms of spontaneous breaking of, respectively, finite *higher-form* and *subsystem symmetries* [25–27]. This follows from the definition of topological order in terms of local indistinguishability of ground states [28, 29]. Additionally, any two ground states are connected by *extended* symmetry operators, which precisely fits the notion of spontaneous symmetry breaking in the context of a generalized symmetry [30]. Generalized symmetries appear to distinguish themselves from usual symmetries, as they can be present in low-energy states even when the Hamiltonian is not symmetric [30–32]. Furthermore, although in this work we only discuss systems containing Abelian anyons—usually associated to higher-form and subsystem symmetries—it is worth mentioning that non-Abelian anyons can also be casted in the language of generalized *non-invertible* symmetries [33–37].

An alternative way of understanding the nontriviality of the ground state space is through the nontrivial braiding statistics among excitations, which signals the presence of 't Hooft anomalies in Abelian topological order. The matching of anomalies from the ultraviolet (UV) to the infrared (IR) imply that the ground state must be nontrivially gapped [38].

It is common for d-dimensional systems invariant under subsystem symmetries, with support in dimensions smaller than d, to have a subextensive number of conserved charges. Typical examples are type-I fracton systems that, when defined on a $3d$ $L\times L\times L$ system, possess charge conservation laws in $O(L)$ individual planes [14,15]. This leads to a macroscopically large amount of symmetry generators, which in turn implies an enormous degeneracy of states. In particular, the ground state degeneracy (IR feature) is sensitive to the number of sites of the system (UV feature)—a phenomenon called UV/IR mixing.

The emergence of UV/IR mixing from simple bosonic local theories has challenged our understanding of effective theories and renormalization group. This follows from the fact that the IR physics depends sensitively on the UV details of the theory, and has been a major point of investigation [12, 39–42]. In the context of generalized symmetries, several exactly solvable models have shed light on the origin of such phenomenon. In the context of gapped dipole moments (and higher-multipole momenta) conserving gauge theories, emergent higher-form symmetries obey twisted boundary conditions in order for holonomy operators to close onto themselves [43–46]. For subsystem symmetries, which are closely related with systems studied in the work, the UV/IR mixing emerges from the fact that the system possesses an increasing number of symmetries as the system size grows [3, 16, 47].

A more dramatic manifestation of UV/IR mixing shows up in the case of subsystem symmetries where the charges are supported in sub-manifolds of fractal dimensions [39, 48–54]. These symmetries are intimately related to type-II fracton physics [4], where no excitations are allowed to move. In the following sections it will be reported about fractal symmetries with support on Sierpinski triangles, which have Hausdorff dimension $\log(3)/\log(2)$. As a consequence, the low-energy properties are extremely sensitive to the lattice details and typically there is no uniform dependence of the ground state degeneracy with the lattice size as in the case of type-I fractons. Additionally, we find that the fractal symmetries are always broken. Whether it is spontaneously or explicitly broken, depends on the lattice size.

This thesis is based on the paper [55] and an ongoing work. It is organized as follows. First of all, Chapter 2 is dedicated to introducing a model that captures the topologically ordered phase, incorporating fractal subsystem symmetries and ground state degeneracy. Subsequently, in Chapter 3, we present the line and fractal symmetry operators and explore the mixed t' Hooft anomaly. The symmetry operators for non-degenerate system sizes, as well as the mutual statistics of the excitations and the long-range entanglement are discussed in Chapters 4 and 5, respectively. In Chapter 6, we provide an interpretation of the degeneracy observed in the topologically ordered phase as a spontaneous symmetry breaking of the subsystem symmetry. Chapter 7 is dedicated to the physics of the boundary of this system and its correlation with $2d$ models. Following this, in Chapter 8, we construct an effective description of this model and discuss the edge modes. We conclude in Chapter 9 with some final remarks.

2 Topologically Ordered Fractal Phase

The model was originally introduced in the context of fragile quantum glasses [49] and further studied recently in [55]. It is defined in a hexagonal close-packed (HCP) lattice, that is a structure composed by two triangular sublattices, $\Lambda = \Lambda_1 \oplus \Lambda_2$, which are not perfectly aligned. Instead, these sublattices exhibit a relative shift, as depicted in Fig. 1. On this lattice, we define the operators

$$\mathcal{O}_{p,a} \equiv Z_{p+\frac{1}{2}\hat{z}}\, X_{p+\hat{\epsilon}_1^a}\, X_{p+\hat{\epsilon}_2^a}\, X_{p-\hat{\epsilon}_1^a-\hat{\epsilon}_2^a}\, Z_{p-\frac{1}{2}\hat{z}}, \tag{2.1}$$

where X and Z are Pauli matrices, p is the center of the operator, and

$$\hat{\epsilon}_1^a \equiv \frac{1}{2}\hat{x} + (-1)^a \frac{1}{2\sqrt{3}}\hat{y} \quad \text{and} \quad \hat{\epsilon}_2^a \equiv -\frac{1}{2}\hat{x} + (-1)^a \frac{1}{2\sqrt{3}}\hat{y}. \tag{2.2}$$

The index a can assume the values 1 or 2 and corresponds to the respective sublattice Λ_a. In situations where the distinction is not essential, the index a may be omitted. With this definition of $\hat{\epsilon}_i^a$, the operators on the xy-plane of different sublattices point in opposite directions. Figure 1 provides a visual representation of the operator defined in Eq. (2.1), featuring a geometric structure known as a "Triangular Dipyramid" (TD). Thus, we shall refer to such operators as TD operators.

The Hamiltonian is defined as a sum of commuting projectors,

$$H = -J \sum_{a=1,2} \sum_{p\in\Lambda_a} \mathcal{O}_p, \qquad (J > 0), \tag{2.3}$$

what makes it exactly soluble. It is simple to check that $[\mathcal{O}_p, \mathcal{O}_q] = 0$, due to the fact that these operators can either share only one site or two sites, as illustrated in Fig. 2. Given that $(\mathcal{O}_p)^2 = \mathbb{1}$, it follows that the eigenvalues of the TD operators are restricted to ± 1. Consequently, the ground state of the system corresponds to

$$\mathcal{O}_p \left|GS\right\rangle = +1 \left|GS\right\rangle, \quad \text{for all} \quad p. \tag{2.4}$$

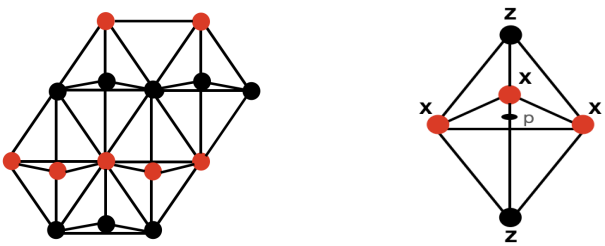

Figure 1 – In the left a representation of hexagonal close-packed lattice and in the right a TD operator.

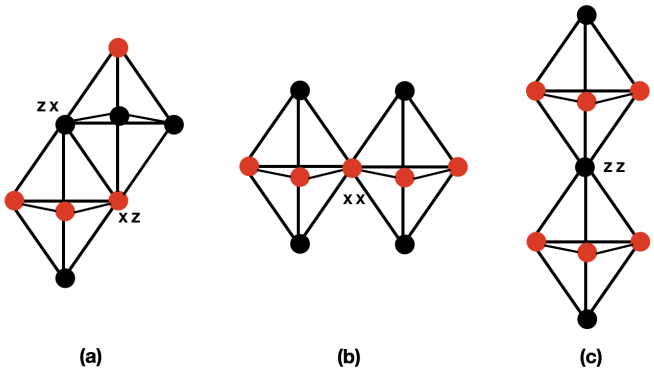

Figure 2 – In (a) the TD operators has two sites in common, whereas in (b) and (c) they share a single site.

2.1 Ground State Degeneracy

Considering periodic boundary conditions (PBC), there is a one-to-one correspondence among spins and TD operators. As a result, the conditions given by Eq. (2.4) label N degrees of freedom on the ground state, except for constraints among the TD operators. Hence, the ground state degeneracy is associated precisely with the number of constraints, N_c, of the system,

$$GSD = \frac{2^N}{2^{N-N_c}} = 2^{N_c}. \tag{2.5}$$

The number of constraints depends dramatically on the linear size of the lattice in the xy-plane, reflecting a strong form of UV-IR mixing. The computation of the ground state degeneracy for linear sizes $L_x = L_y = L$ was presented in [55]. We shall firstly review this intricate computation and then discuss how it can be fully generalized to arbitrary sizes with $L_x \neq L_y$.

2.2 Sizes with $L_x = L_y = L$

The constraints can be expressed in terms of a set $\{t\}$ of variables defined in $\mathbb{Z}_2$ as

$$\prod_p \mathcal{O}_p^{t_p} = \mathbb{1}. \tag{2.6}$$

The number of linearly independent nontrivial solutions of t_p is precisely N_c. This product can be rewrite in the spins lattice $\tilde{\Lambda}$, instead of the original lattice of the operators Λ,

$$\prod_{p\in\Lambda} \mathcal{O}_p^{t_p} = \prod_{j\in\tilde{\Lambda}} Z_j^{t_{p_j-\hat{z}/2}} X_j^{t_{p_j}} X_j^{t_{p_j+\hat{e}_1}} X_j^{t_{p_j+\hat{e}_2}} Z_j^{t_{p_j+\hat{z}/2}} = \mathbb{1}, \tag{2.7}$$

where p_j is a site in $\tilde{\Lambda}$ that corresponds to p in the original lattice[1], as depicted in Fig. 3. Eq. (2.7) leads to two conditions that must be satisfied. From the Z operators, we obtain

$$t_{p_j+\frac{\hat{z}}{2}} + t_{p_j-\frac{\hat{z}}{2}} = 0 \pmod 2 \tag{2.8}$$

[1] We will typically use the i, j, and k for sites in $\tilde{\Lambda}$ and p, and q for sites in Λ.

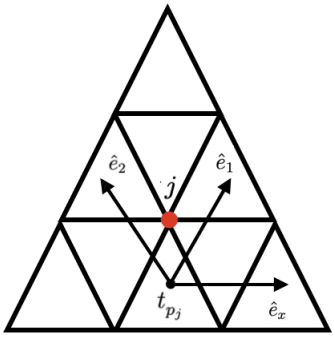

Figure 3 – The xy-plane.

and from the X operators we have

$$t_{p_j} + t_{p_j+\hat{e}_1} + t_{p_j+\hat{e}_2} = 0 \pmod 2. \tag{2.9}$$

Eq. (2.8) implies that all t_{p_j} in a straight line along z-direction must have the same value. Therefore, it is sufficient to consider only two xy-planes, one from each sublattice, to completely define the whole set t.

Eq. (2.9) leads to constraints in each one of the xy-planes, which are closely tied to the fractal features of the model (2.3). To further understand this, it is convenient to adjust the notation and rewrite Eq. (2.9) as

$$t_{j+1,i} = t_{j,i} + t_{j,i-1} \pmod 2, \tag{2.10}$$

where i and j denote orthogonal directions in the plane, as illustrated in Fig. 4. As discussed in [52], in the context cellular automaton, this equation defines a Sierpinski rule. It works as a "translationally-invariant local linear update rule", in the sense that a state can be determined by the configuration of the previous time step. In the present case, this constraint has a similar role. Given a line configuration[2] $\{t_{j,i}\}$, Eq. (2.10) allows us to fully determine the subsequent line $\{t_{j+1,i}\}$ and, consequently, the entire plane.

To find the constraints in the xy-plane, we will introduce a polynomial representation [52]. A line configuration can be represented by a Laurent series as

$$S_j(x) = \sum_{i=1}^{L} t_{j,i}\, x^i, \tag{2.11}$$

where the coefficients are the variables $t_{j,i}$ defined mod 2. By incorporating into this definition the update rule (2.10), we obtain

$$S_{j+1}(x) = \sum_{i=1}^{L} (t_{j,i} + t_{j,i-1})\, x^i = (1+x)\, S_j(x), \tag{2.12}$$

[2] In this context we will use the term "configuration" to represent the arrangement of the variables $t_{j,i}$.

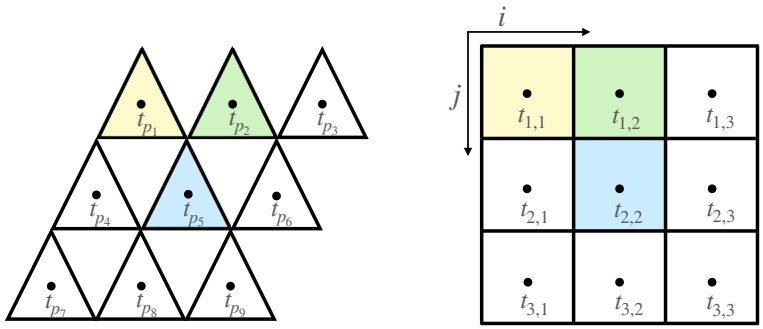

Figure 4 – In Figure (a) the t_{p_j} are represented in the original triangular lattice, and in Figure (b) the positions new notation of $t_{j,i}$.

where $(1+x)$ is the polynomial representation of the Sierpinski evolution. Given an initial line configuration $S_1(x)$, any subsequent line $S_{j+1}(x)$ can be determined recursively applying Eq. (2.12), resulting in

$$S_{j+1}(x) = (1+x)^j S_1(x). \tag{2.13}$$

When the Sierpinski evolution is compatible with PBC, the product of TD operators arranged in a fractal structure results in an identity, leading to certain constraints among $\mathcal{O}_p$'s in the xy-plane. In terms of the polynomial representation, PBC translate into $S_{j+L}(x) = S_j(x)$ and $x^{i+L} = x^i$. Therefore, our goal is to identify configurations $S_1(x)$ that satisfy the condition

$$S_{1+L}(x) = (1+x)^L S_1(x) = S_1(x). \tag{2.14}$$

With this purpose, we note that $S_1(x)$ must contain an even number of non-zero $t_{1,i}$'s to be compatible with PBC. This requirement becomes evident by considering a simple configuration $S_1(x) = x^i$. Then, the evolution governed by (2.13) implies that all subsequent lines $S_j(x)$ have an even number of $t_{j,i} \neq 0$. Consequently, it becomes impossible to find $S_{L+1} = x^i$, to satisfy the PBC.

For a consistent first line configuration consider

$$S_1(x) = (1+x)^{2^m} \sum_{i=1}^{L} t_{1,i}\, x^i, \tag{2.15}$$

with $m = 0, 1, 2, \ldots$. The term included in this equation follows the "Freshman's dream",

$$(1+x)^{2^m} = 1 + x^{2^m} \pmod 2 \tag{2.16}$$

for any integer m, and ensures an even number of non-zero coefficients. This result follows from the binomial expansion,

$$(1+x)^{2^m} = \sum_{l=0}^{2^m} \binom{2^m}{l} x^l, \tag{2.17}$$

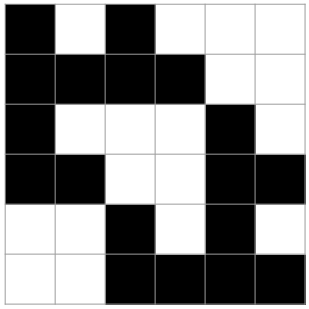

Figure 5 – Example of a configuration generated by Eq. (2.20) in a lattice of size 6×6

where the binomial coefficient is even for any l, except when l equals to 0 or 2^m. The configuration defined in Eq. (2.15), under periodic boundary conditions, implies

$$S_{L+1}(x) = (1+x)^{L+2^m} \sum_{i=1}^{L} t_{1,i}\, x^i = (1+x)^{2^n} \sum_{i=1}^{L} t_{1,i}\, x^i. \tag{2.18}$$

Consequently, any linear size of the form

$$L \equiv 2^n - 2^m, \qquad n > 2 \quad \text{and} \quad 0 \leq m < n-1, \tag{2.19}$$

has constraints in the xy-plane generated by

$$S_1(x) = (1+x)^{2^m} \sum_{i=1}^{L} t_{1,i}\, x^i. \tag{2.20}$$

An example of a configuration generated by (2.20) is shown in Fig. 5.

To specify all possible configurations of the set $\{t\}$, we can define the basis elements as

$$S_1^i(x) = \left(1 + x^{2^m}\right) x^i, \qquad \text{for} \quad i = 1, 2, \ldots, 2^n - 2^{m+1}. \tag{2.21}$$

This basis defines the dimension of the set of first lines as $2^n - 2^{m+1}$ for each plane (in the Supplementary Material A we have included some examples to illustrate this discussion). Equation (2.8) defines two independent planes, so N_c is twice the constraints of a single plane. As discussed in Eq. (2.5), the degeneracy corresponds precisely to N_c. Therefore, a size $L = 2^n - 2^m$ has a ground state degeneracy of

$$GSD = 2^{2^{n+1} - 2^{m+2}}. \tag{2.22}$$

For sizes which are not of the form (2.19), the ground state is unique.

2.3 Sizes with $L_x \neq L_y$

We discuss now the generalization of the previous computation for cases with $L_x \neq L_y$. There are some compatibility conditions for the sizes L_x and L_y in such a way that the system can exhibit nontrivial ground state degeneracy. When at least one

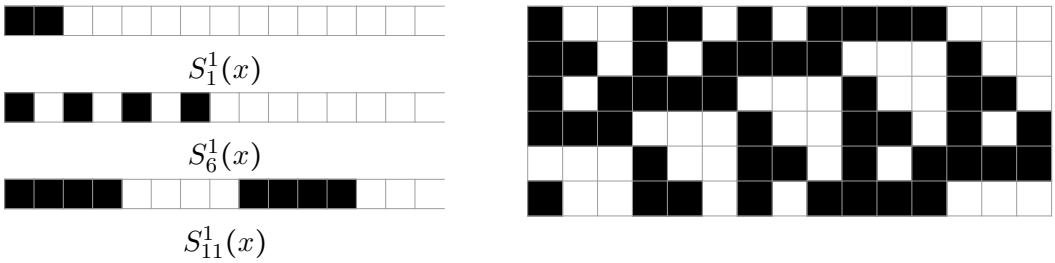

Figure 6 – For $L_y = 5$ and $L_x = 15$, defining $\bar{S}_1^1(x) = S_1^1(x) + S_6^1(x) + S_{11}^1(x)$, the first line respects $\bar{S}_1^1(x) = \bar{S}_6^1(x)$. On the left it shows $S_1^1(x)$, $S_6^1(x)$, and $S_{11}^1(x)$, and on the right is depicted a 15×5 configuration (the first and de last rows are the same).

of the linear sizes is not of the form (2.19), the ground state is unique. Assuming that $L_x = 2^n - 2^m$, we will show that the system supports a degenerate ground state if L_y is a divisor of L_x, i.e., $L_x = rL_y$, for positive integers r.

To understand this, we notice that the first line configuration $S_1^i(x)$, as defined in Eq. (2.21), does not respect the perodicity in the y-direction, $S_{1+L_y}^i(x) \neq S_1^i(x)$. However, we can use it to construct another first line configuration that has the proper periodicity,

$$\bar{S}_1^i(x) \equiv \sum_{l=0}^{r-1} (1+x)^{lL_y} \left(1 + x^{2^m}\right) x^i, \tag{2.23}$$

where $i = 1, 2, \ldots, 2^n - 2^{m+1}$. Now we proceed to check that this configuration indeed satisfies the PBC $\bar{S}_{1+L_y}^i(x) = \bar{S}_1^i(x)$. We can write

$$\bar{S}_{1+L_y}^i(x) = (1+x)^{L_y} \bar{S}_1^i(x) = \sum_{l=1}^{r} (1+x)^{lL_y} S_1^i(x). \tag{2.24}$$

In the element of the sum with $l = r$, it is possible to use the property (2.16) and the fact that $rL_y = L = 2^n - 2^m$, to write

$$\begin{aligned} (1+x)^{rL_y} S_1^i(x) &= (1+x)^{2^n} x^i = \left(1 + x^{2^n}\right) x^i \\ &= \left(1 + x^{L+2^m}\right) x^i = \left(1 + x^{2^m}\right) x^i \\ &= (1+x)^{2^m} x^i = S_1^i(x). \end{aligned} \tag{2.25}$$

Consequently, we find

$$\begin{aligned} \bar{S}_{1+L_y}^i(x) &= \sum_{l=1}^{r} (1+x)^{lL_y} S_1^i(x) \\ &= \sum_{k=0}^{r-1} (1+x)^{lL_y} S_1^i(x) = \bar{S}_1^i(x). \end{aligned} \tag{2.26}$$

In Fig. 6, we show an example of $\bar{S}_1^i(x)$ for $L_x = 15$ and $L_y = 5$.

We can determine the number of independent first line configurations directly from (2.23), which corresponds to the maximum value of i before it starts to repeat under PBC. It is given by

$$i_{max} = L_y - 2^m. \tag{2.27}$$

However, we need some attention to use correctly this result. This is so because it may happen that

$$L_x = kL'_x, \tag{2.28}$$

with $L_x = 2^n - 2^m$, $L'_x = 2^{n'} - 2^{m'}$, and k a positive integer. Then we can write

$$\begin{aligned} L_x \times L_y &= L_x \times \frac{L_x}{r} \\ &= kL'_x \times \frac{kL'_x}{r} \\ & kL'_x \times \frac{L'_x}{r'}, \end{aligned} \tag{2.29}$$

where $r' \equiv \frac{r}{k}$ must be a positive integer[3]. Notice that L_y is preserved under such redefinitions, i.e., $L_y = \frac{L_x}{r} = \frac{L'_x}{r'}$. In this case, the maximum number of independent first line configurations is dictated by the smallest value among m and m'. For example, consider a system 14×7, whose linear size in the x-direction can be written as $2^n - 2^m = 2^4 - 2^1$ or $k(2^{n'} - 2^{m'}) = 2(2^3 - 2^0)$. The maximum number of independent first line configurations is given by (2.27) with $L_y = 7$ and $m' = 0$, which leads to $7 - 1 = 6$. Therefore, the building-block associated with the zise 14×7 is that one of size 7×7.

Using this reasoning, we can understand that all the cases where $L_y < 2^m$ so that (2.27) would lead to a negative value are actually constructed from smaller building-block sizes. To see this, we parametrize the divisors of $L_x = 2^n - 2^m = 2^m(2^{n-m} - 1)$ as

$$r(l, q) = 2^l q, \tag{2.30}$$

where q is a divisor of $2^{n-m} - 1$ and $l = 1, \ldots, m$. Note that as $2^{n-m} - 1$ is an odd number, then the maximum value of q is $(2^{n-m} - 1)/2$. Now, the condition $L_y < 2^m$ can be written as $r(l, q) > 2^{n-m} - 1$, which implies

$$2^l > 2 \quad \Rightarrow \quad l > 1. \tag{2.31}$$

Thus we can re-express

$$\begin{aligned} L_x \times L_y &= (2^n - 2^m) \times \frac{(2^n - 2^m)}{2^l q} \\ &= 2^l(2^{n-l} - 2^{m-l}) \times \frac{(2^{n-l} - 2^{m-l})}{q} \\ &= k(2^{n'} - 2^{m'}) \times \frac{2^{n'} - 2^{m'}}{r'} \\ &= kL'_x \times L_y, \end{aligned} \tag{2.32}$$

where $k \equiv 2^l$, $n' \equiv n - l$, $m' \equiv m - l$, and $r' = q$. As $m > m'$, then the number of linearly independent first line configurations is dictated by $L_y - 2^{m'} > 0$. As an example, let us

[3] As both r and k are divisors of L_x, there is at least one value of k so that $r' = \frac{r}{k}$ is a positive integer, namely, $k = r$.

System Size	$\log_2(GSD)$
$L_x, L_y \neq k(2^n - 2^m)$	0
$L_x = k(2^n - 2^m)$, $L_y \neq \frac{L_x}{r}$	0
$L_x = k(2^n - 2^m)$, $L_y = \frac{L_x}{r}$	$2\,(L_y - 2^m)$

Table 1 – Ground state degeneracy depending on the system size. When there are different ways to decompose L_x in the form $L_x = k(2^n - 2^m)$ satisfying the requirement that $r' = \frac{r}{k}$ is a positive integer, then the ground state degeneracy is dictated by the decomposition corresponding to the smallest value of m.

consider a system with size 24×6, which gives $r = 4$. We first note that 24 is of the form $2^n - 2^m$, namely, $24 = 2^5 - 2^3$. A naive application of (2.27) leads to $i_{max} = 6 - 2^3 = -2$. However, the linear size along the x-direction can be decomposed in the form (2.28) in several ways

$$\begin{aligned} 24 &= 2(2^4 - 2^2) \\ &= 3(2^4 - 2^3) \\ &= 4(2^3 - 2^1) \\ &= 6(2^3 - 2^2) \\ &= 8(2^2 - 2^0) \\ &= 12(2^2 - 2^1). \end{aligned} \tag{2.33}$$

The only decompositions which keep L_y invariant, i.e., that ones with $r' = \frac{r}{k}$ being a positive integer, are $2(2^4 - 2^2)$, with $k = 2$, $r' = 2$, and $m = 2$; and $4(2^3 - 2^1)$, with $k = 4$, $r' = 1$, and $m = 1$. As $m = 1 < m = 4$, the maximum number of independent first line configurations is dictated by the decomposition $24 = 4(2^3 - 2^1)$, which leads to $6 - 2^1 = 4$. The results for the ground state degeneracy depending on the system are summarized in Table 1.

Finally, we note that the sizes in Table (1) can be used as building-blocks for sizes $k_i(L_x \times L_y)$, where k_b, $b = x, y$, is a positive integer with the subscript $b = x, y$ indicating in which direction the copies are disposed. The ground state degeneracy is dictated by the building-block $L_x \times L_y$. As an example, consider the size 30×20. It is not of the form of the sizes present in the Table 1, but it can be written as $2_y(30 \times 10)$, where 2_y means that the two copies are disposed along the y-direction.

3 Symmetry Operators and Mixed 't Hooft Anomalies

The ground state degeneracy is closely connected with the symmetry operators and their anomalies. For degenerated system sizes, the model defined in (2.3) exhibits two distinct types of symmetry: Wilson lines and Fractal membranes. The Wilson lines are represented by closed loops in the z-direction, while fractal symmetries manifest as closed membranes in the xy-plane. Both symmetries - line and membrane - are mutually anomalous, implying a nontrivial degeneracy. In non-degenerated system sizes, the fractal membranes fail to close properly, resulting in the explicit breaking of fractal symmetry due to the system size.

3.1 Wilson Lines

The Wilson line operators are products along the z-direction, given by

$$W_i^a = \prod_{j \in \mathcal{L}_i^a} X_j, \tag{3.1}$$

where $\mathcal{L}_i^a$ defines a straight line across all xy-planes at the point $i = (x, y)$ belonging to the sublattice a. Under PBC, it forms a closed loop and hence corresponds to a nontrivial symmetry of the Hamiltonian.

There is one different W_i^a operator for each point i on the xy-plane, resulting in a total of $L_x L_y$ operators. However, not all of them are independent. A number of constraints arises from the fact that the product of TD operators along a straight line in the z-direction is equivalent to the product of three Wilson lines,

$$\prod_{p \in \mathcal{L}_q^a} \mathcal{O}_p = W_i^a W_j^a W_k^a. \tag{3.2}$$

This is illustrated in Fig. 7. As there is a one-to-one correspondence between points of the dual and original lattices, there are $L_x L_y$ constraints, but not all of them are independent because the topological constraints discussed in Sec. 2.1, which can be expressed as

$$\prod_z \prod_{p \in \mathcal{M}_I^a(z)} \mathcal{O}_p = \prod_{q \in \mathcal{M}_I^a} \prod_{p \in \mathcal{L}_q^a} \mathcal{O}_p = \mathbb{1}, \tag{3.3}$$

where $\mathcal{M}_I^a$, $I = 1, 2, \ldots, L_y - 2^m$, represents a configuration of TD operators in the xy-plane corresponding to a constraint. Putting apart one point p' from this product we find

$$\left(\prod_{p \in \mathcal{L}_{p'}^a} \mathcal{O}_p \right) \prod_{\substack{q \in \mathcal{M}_I^a \\ q \neq p'}} \prod_{p \in \mathcal{L}_q^a} \mathcal{O}_p = \mathbb{1} \qquad \Rightarrow \qquad \prod_{\substack{q \in \mathcal{M}_I^a \\ q \neq p'}} \prod_{p \in \mathcal{L}_q^a} \mathcal{O}_p = W_i^a W_j^a W_k^a. \tag{3.4}$$

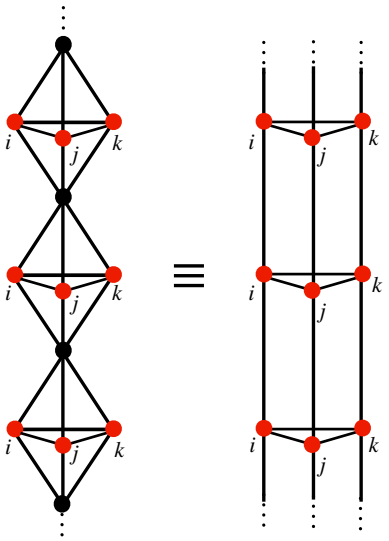

Figure 7 – The product of TD operators along the z-direction, reducing to the product of three Wilson lines.

Equation (3.4) reveals that one of the constraints defined in Eq. (3.2) can be expressed in terms of the others. This process can be repeated for all the $N_c = L_y - 2^m$ constraints, so that the total number of independent W_I^a is precisely $L_x L_y - (L_x L_y - N_c) = N_c$. For this reason, we will label the independent Wilson lines with the index I,

$$W_I^a \equiv \prod_{j \in \mathcal{L}_I^a} X_j \,, \qquad I = 1, 2, \ldots, N_c \,. \tag{3.5}$$

For system sizes with a unique ground state, there are no independent Wilson lines. In these cases, all W_i^a can be reduced to a product of TD operators and, consequently, they represent trivial symmetries.

3.2 Fractal Membranes

For a system size with a degenerated ground state, the fractal membrane operators are closely related to the topological constraints. Rewriting the constraint equation

$$\prod_z \prod_{p \in \mathcal{M}_I^a(z)} \mathcal{O}_p = \mathbb{1}, \tag{3.6}$$

we note that a subset of this product, ranging from $z_1 + a_0/2$ to $z_2 - a_0/2$, results in one membrane at the bottom and other membrane at the top of this product in z,

$$\prod_{z=z_1-\frac{a_0}{2}}^{z_2+\frac{a_0}{2}} \prod_{p \in \mathcal{M}_I^a(z)} \mathcal{O}_p = M_I^b(z_1)\, M_I^b(z_2), \qquad b \neq a, \tag{3.7}$$

where we have define the fractal membrane operator as

$$M_I^b(z) \equiv \prod_{j \in \mathcal{M}_I^b(z)} Z_j. \tag{3.8}$$

Note that the product of TD operators on the sublattice a results in Z-operators acting non-trivially on the opposite sublattice. The left-hand side of Eq. (3.7) trivially commutes with the Hamiltonian, since it is simply a product of TD operators, so the product of membrane operators in the right-hand side must do so too. However, the two membranes do not act on the same set of operators and, consequently, each one of them must commute individually with each $\mathcal{O}_p$. Therefore, M_I^b is a nontrivial symmetry. This occurs because the membranes have either zero or two Z_j operators acting non-trivially on each TD operator.

Following the definition in Eq. (3.8), there are N_c independent fractal membrane operators, one for each constraint. Notice that given a membrane $M_I^b(z_1)$, we can move it to z_2 with a product of TD operators,

$$M_I^b(z_1)\left(\prod_{z=z_1-\frac{a_0}{2}}^{z_2+\frac{a_0}{2}}\prod_{p\in\mathcal{M}_I^a}\mathcal{O}_p\right)=M_I^b(z_2). \tag{3.9}$$

If there is no defect between z_1 and z_2, both membranes are constrained to have the same eigenvalue. Due to this mobility, we do not need to specify their position in z.

For the cases where the ground state is unique, there are no topological constraints and, accordingly, there are no fractal membrane operators. This occurs because the fractal structures do not close properly under PBC, indicating that the fractal symmetry is explicitly broken by the lattice size.

3.3 Mixed 't Hooft Anomaly

As discussed earlier, for degenerated system sizes, there is one Wilson line and one fractal membrane associated with each constraint. The pairs of W_I^a and M_I^a can be arranged to satisfy the commutation relation

$$W_I^a M_J^b=(-1)^{\delta_{IJ}\,\delta_{ab}}\,M_J^b W_I^a. \tag{3.10}$$

For each membrane generated by $S_1^i(x)$, as defined in (2.21), there is an specific point with $t_{ij}=1$ that does not repeat for the other membranes. However, using $S_1^i(x)$ makes it nontrivial to identify these unique points. To address this, we introduce a modified basis

$$\tilde{S}_p^l\equiv\sum_{i=1}^{l}S_1^{2^m i-p}, \tag{3.11}$$

where $p=0,1,2,\ldots,2^m-1$, and $l=1,2,\ldots,2^n-2^{m+1}/2^m$. This redefinition ensures that all $t_{ij}=1$ points, which do not repeat for the other membranes, are located in the first line, as depicted in Fig. 8.

With Eq. (3.11), we define $\mathcal{M}_I^a$ as the set $\{t\}$ associated with the Sierpinski fractal structure generated by the first line $\tilde{S}_1^I(x)$. Similarly, $\mathcal{L}_I^a$ is defined as the straight line

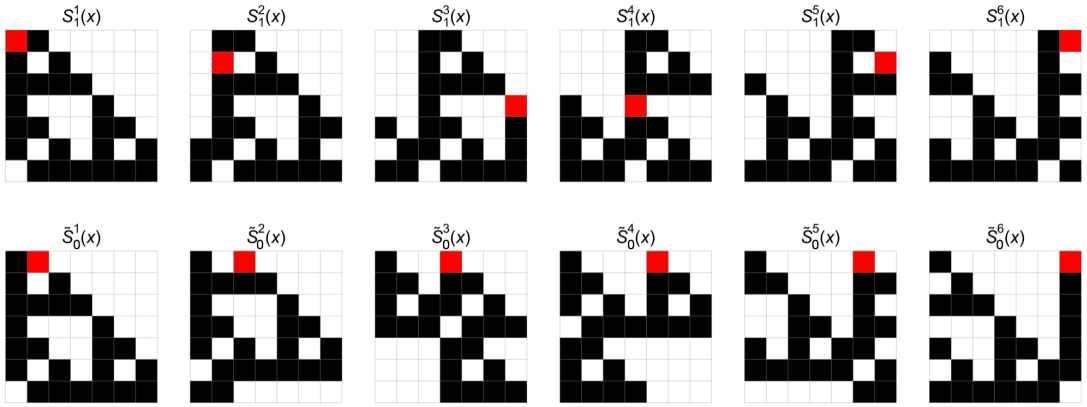

Figure 8 – The membranes generated by $S_1^i(x)$ and $\tilde{S}_1^i(x)$, where $i = 1, 2, \ldots, 6$, in system of size $L = 7$. Each membrane highlights the unique $t_{ij} = 1$ that do not repeat in other membranes.

along the z-direction that touches only the respective $\mathcal{M}_I^a$. Consequently, the definitions of the symmetry operators in (3.5) and (3.8) automatically respect the commutation in Eq. (3.10), corresponding to a projective realization of the subsystem symmetries.

This nontrivial algebra implies that the eigenstates of the Hamiltonian can be eigenstates of either W_I^a but not both simultaneously. Accordingly, there is a $2^{2(2^n-2^m)}$ degeneracy in the states, precisely matching Eq. (2.5). This algebra can also be understood as a mixed 't Hooft anomaly among the symmetries, preventing the ground state from being trivially gapped.

4 Non-degenerate Cases

For system sizes that do not fit $L = k\,(2^n - 2^m)$there are no topological constraints ($N_c = 0$), and the system is non-degenerate. In these cases, the fractal membranes do not close properly; consequently, there are no membrane symmetry operators, and the fractal symmetry is explicitly broken by the lattice size.

For these sizes it also occurs that the Wilson lines are trivial symmetries, as they reduce to a product of TD operators. Consider a product of TD operators in a set $\tilde{M}_I^a$ that reduces to identities at every site except for one, resulting in an X_k,

$$\prod_{p\in\tilde{\mathcal{M}}_k^a(z)} \mathcal{O}_p = X^k \prod_{i\in\tilde{\mathcal{M}}_k^a(z+\frac{1}{2})} Z_i \prod_{i\in\tilde{\mathcal{M}}_k^a(z-\frac{1}{2})} Z_i. \tag{4.1}$$

Then, stacking this product along the z-direction results precisely in the Wilson line,

$$\prod_z \prod_{p\in\tilde{\mathcal{M}}_k^a(z)} \mathcal{O}_p = \prod_{i\in\mathcal{L}_k^a} X^i = W_k^a. \tag{4.2}$$

In order to find $\tilde{M}_I^a$ we need to discuss the configurations of $\{t\}$ again. As discussed earlier for the constraints, given any $S_1(x)$ configuration, the Sierpinski evolution ensures that the product of $\mathcal{O}_j$ reduces to identities in the intersection of two subsequent lines, $S_i(x)$ and $S_{i+1}(x)$. Therefore, for a given $S_1(x)$ that satisfies

$$S_1(x) + S_{1+L}(x) = x^j \tag{4.3}$$

under the Sierpinski evolution, we can properly generate a set $\tilde{\mathcal{M}}_k^a$ that results in a single X_k on the plane. In Fig. 9 we depict the product of $\mathcal{O}_p$ over a plane for some of these sizes, such that the result is a single X_k. Stacking this structure along the z-direction results precisely in a Wilson line.

The first line configuration that gives rise to $\tilde{\mathcal{M}}_k^a$ is constructed by finding the coefficients $t_{1,i}$ that satisfy

$$\begin{aligned} S_1(x) + S_{1+L}(x) &= \left[1 + (1+x)^L\right] S_1(x) \\ &= \sum_{i=1}^{L}\sum_{j=1}^{L} \binom{L}{j} t_{1,i}\, x^{i+j} = x^k. \end{aligned} \tag{4.4}$$

It is useful to rewrite the sum in the last equation as

$$\begin{aligned} \sum_{i=1}^{L}\sum_{j'=i+1}^{i+L} t_{1,i}\binom{L}{j'-i} x^{j'} &= \sum_{i=1}^{L}\left(\sum_{j'=i+1}^{L}\binom{L}{j'-i} t_{1,i}\, x^{j'} + \sum_{j'=L+1}^{i+L}\binom{L}{j'-i} t_{1,i}\, x^{j'-L}\right) \\ &= \sum_{i=1}^{L}\left(\sum_{j'=i+1}^{L}\binom{L}{j'-i} t_{1,i}\, x^{j'} + \sum_{j'=1}^{i}\binom{L}{j'+L-i} t_{1,i}\, x^{j'}\right) \\ &= \sum_{i=1}^{L}\sum_{j=1}^{L}\binom{L}{|i-j|} t_{1,i}\, x^{j}, \end{aligned} \tag{4.5}$$

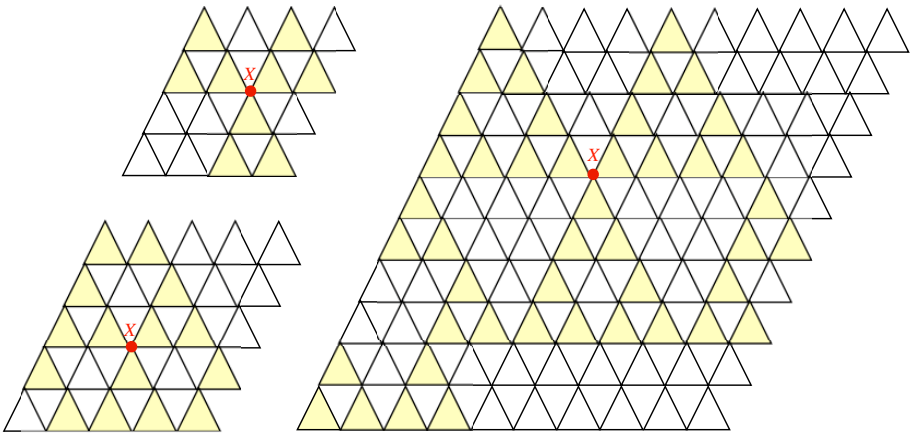

Figure 9 – For non-degenerated system sizes, a single X_k operator can be obtained by the product of TD operators over a plane. The figures above depict this product for $L = 4$, $L = 5$, and $L = 10$.

in which we defined $j' = i + j$, and used the identification $x^{j'+L} = x^{j'}$. In the last step, we have also used the binomial identity $\binom{L}{L-a} = \binom{L}{a}$. It results in

$$\sum_{i=1}^{L}\sum_{j=1}^{L}\binom{L}{|i-j|}t_{1,i}\,x^{j} = x^{k} \pmod 2 \tag{4.6}$$

and the coefficients of $S_1(x)$ are the solution of

$$\sum_{i=1}^{L}\binom{L}{|i-j|}t_{1,i} \bmod 2 = \begin{cases} 1 & \text{if} \quad j = k, \\ 0 & \text{otherwise.} \end{cases} \tag{4.7}$$

We have found in Eq. (4.7) a system of L equations, with coefficients $\binom{L}{|i-j|}$ and variables $t_{1,i}$. Expressing it in matrix form, where the elements are $M_{ij} = \binom{L}{|i-j|} \bmod 2$, results in an $L \times L$ circulant matrix. For any system size L such that $\det M \neq 0$, this system has a non-trivial solution, and it is straightforward to determine $S_1(x)$.

For these system sizes it also occurs that it is possible to create a localized excitation. Following the same strategy to construct the membrane symmetry operators (see Sec. 3.2) but with $\tilde{\mathcal{M}}_i^a$ instead of a constraint results in a membrane operator that excites a single TD operator,

$$\prod_{j\,\in\,\tilde{\mathcal{M}}_I^b(z)} Z_j \equiv \tilde{M}_I^b(z). \tag{4.8}$$

The fact that a single excitation can be created implies that there is only one global anyonic superselection sector.

5 Excitations and Mutual Statistics

An excitation, or defect, corresponds to any $\mathcal{O}_p$ with eigenvalue -1. The action of an X_j on the ground state creates a state with two excitations, while a Z_j is responsible for creating three excitations. Open Wilson lines create a pair of excitations, one at each end-point, and can move a single excitation along the z-direction. Analogously, three excitations can be separated through the action of open membranes, with some restrictions on the end position due to the fractal structure. However, this *mobility* in the xy-plane occurs by crossing highly energetic virtual states, making the probability of tunneling very small. This is the reason behind the type-II fractonic behavior, the excitation are effectively immobile on the xy-planes.

Note that, considering open operators M_I^a and W_I^a, while the membrane moves charges in the sublattice a, the Wilson line moves charges of the other sublattice. Despite the mobility in the plane or in the z-direction, the excitations cannot be moved from one sublattice to the other. This leads us to interpret them as two distinct types of excitations[1].

It is intriguing that even with only short-range interaction, the low energy states of (2.3) are highly entangled. One evidence of the long-ranged entanglement is the property of the state to acquire a phase through the movement of the excitations, even if they never touch each other. This phenomenon becomes apparent when we examine specific sequences of movements. Consider a state represented by $|a_3, b_2\rangle$ containing three excitations in sublattice a (created by Z_j operators) and, situated far apart, a pair of excitations in sublattice b (created by an X_j), with $b \neq a$.

In this scenario, we initiate the movement of excitations as follows: firstly, we move one excitation from sublattice b using an open Wilson line W_I^a; subsequently, we separate the trio in sublattice a using an open membrane M_I^a; next, we return the excitation in sublattice b to its original position with $W_I^{a\dagger}$; and finally, we restore the trio in sublattice a to its initial state with $M_I^{a\dagger}$. throughout this procedure, the excitations of sublattice a and b never touch, but the movement of b excitation along the z-direction leads it to cross the membrane M_I^a, as illustrated in Fig. 10.

Algebraically, this procedure can be expressed as

$$M_I^{a\dagger}\, W_I^{a\dagger}\, M_I^a\, W_I^a\, |a_3, b_2\rangle = -\,|a_3, b_2\rangle \tag{5.1}$$

where we use the fact that $W_I^{a\dagger}\, M_I^a = -M_I^a\, W_I^{a\dagger}$. The acquired phase on the right-hand side signifies a mutual anyonic statistics among the excitations, a marker of the long-range entanglement inherent in topologically ordered phases.

[1] The Hamiltonian (2.3) could be equivalently constructed in therms of TD operators defined as a product of only X_j in one sublattice and as a product of only Z_j in the other. In this notation, one could refer to them as electric or magnetic excitations depending on their sublattices, in analogy with the toric code.

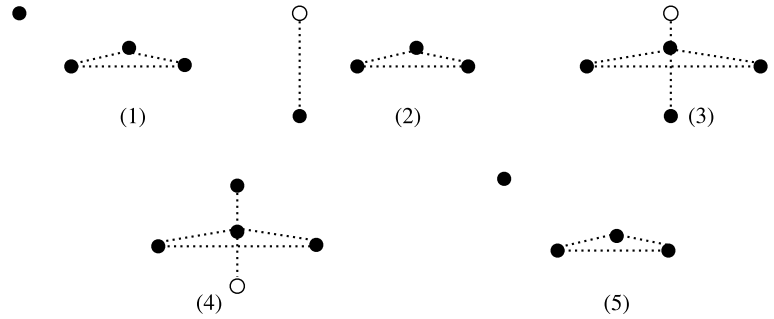

Figure 10 – Sequence of movements reflecting mutual statistics among excitations.

It is important to highlight some details when the ground state is non-degenerated. For these system sizes, the unique global anyonic superselection sector implies that the excitations are bosons. Instead of applying W_I^a and $W_I^{a\dagger}$ in Eq. (5.1), we can "*move*" the excitation with two $\tilde{M}_I^a$, annihilating it and creating it in another point. This procedure leads to a trivial statistics, as expected for bosonic excitations (since $\left[M_I^a, \tilde{M}_I^a\right] = 0$).

Despite this *global* characteristic, the procedure described in Eq. (5.1) remains valid, and *locally* the excitations behave like anyons. Moreover, the mutual statistics occur for excitations arbitrarily far apart, implying long-range entanglement. Consequently, even when the ground state is non-degenerated, and the fractal symmetry is explicitly broken by the lattice size, the phase is topologically ordered.

6 Spontaneous Breaking of Subsystem Symmetries

It is very instructive to study the fractal topological phases from the perspective of the spontaneous breaking of sub-system symmetries. For system sizes with degeneracy, in each subsystem, we can simultaneously diagonalize one of the symmetry operators with the Hamiltonian, namely

$$H\,|E,\alpha\rangle = E\,|E,\alpha\rangle \qquad \text{and} \qquad W\,|E,\alpha\rangle = \alpha\,|E,\alpha\rangle\,. \tag{6.1}$$

Since $W^2 = \mathbb{1}$, the eigenvalues are constrained to $\alpha = \pm 1$. However, these states are not eigenstates of M (assuming $MW = -WM$), instead, $M\,|E,\alpha\rangle = |E,-\alpha\rangle$ is an orthogonal state,

$$\langle E,\alpha|\,W\,|E,-\alpha\rangle = -\alpha\,\langle E,\alpha|E,-\alpha\rangle = \alpha\,\langle E,\alpha|E,-\alpha\rangle = 0. \tag{6.2}$$

Because W and M are symmetries of the ground state, we say that the subsystem symmetry is spontaneously broken.

The ground state of these topologically ordered phase are characterized by extended operators, and are indistinguishable by any local operator Φ,

$$\langle GS,\alpha|\,\Phi\,|GS,\beta\rangle = C\delta_{\alpha\beta} \tag{6.3}$$

in which C is a constant independent of α and β. In order to check this property, firstly, note that we can always avoid M to touch Φ, since we can move M in z-direction. It implies that M commutes with Φ, and then

$$\begin{aligned}\langle GS,\alpha|\,\Phi\,|GS,\alpha\rangle &= \langle GS,-\alpha|\,M^\dagger\Phi M\,|GS,-\alpha\rangle \\ &= \langle GS,-\alpha|\,\Phi\,|GS,-\alpha\rangle\,.\end{aligned} \tag{6.4}$$

To complete the demonstration of the topological indistinguishably, Eq. (6.3), we need to discuss the deformation of the Wilson lines. This extended operators are not topological deformable because they are rigid, however, they are locally splittable. As demonstrated in Fig. 11, we can construct an operator $\tilde{W} \equiv W\mathcal{O}$ that avoid the position of Φ, and, consequently, $\left[\tilde{W},\Phi\right] = 0$. We can now show that

$$\begin{aligned}\langle GS,-\alpha|\,\Phi\,|GS,\alpha\rangle &= -\alpha\,\alpha\,\langle GS,-\alpha|\,\tilde{W}^\dagger\,\Phi\,\tilde{W}\,|GS,\alpha\rangle \\ &= -\langle GS,-\alpha|\,\Phi\,|GS,\alpha\rangle\,,\end{aligned} \tag{6.5}$$

therefore, $\langle GS,-\alpha|\,\Phi\,|GS,\alpha\rangle = 0$.

The mixed t' Hoof anomaly among the symmetries is responsible for Eq. (6.4) and Eq. (6.5), that implies the locally indistinguishable, Eq. (6.3). Equivalently, the subsystem symmetry are spontaneously broken.

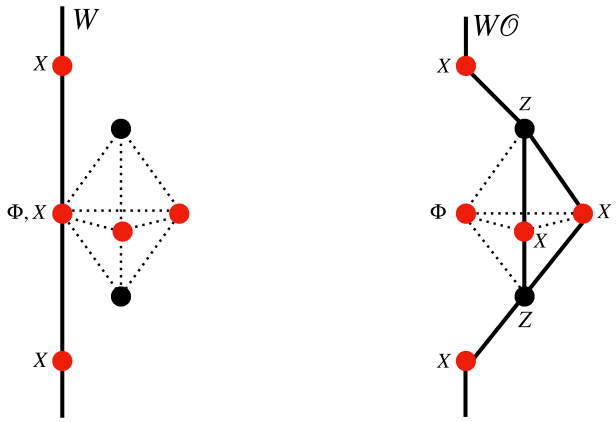

Figure 11 – Local splitability of the Wilson line.

7 Boundary Theory

Consider the Hamiltonian (2.3) in topology with boundaries in z-direction. The ground state degeneracy is drastically affected by the presence of these boundaries. Basically, the GSD is not 2^{N_c} anymore because the number of spin sites is greater than the number of TD operators. For boundaries in z-direction this difference is exactly $2L^2$, one extra spin site for each point of the xy-planes, for each sublattice.

The degeneracy at the boundaries is associated with new symmetry operators. For any sum of commuting projector it is possible to define "truncated" operators at the boundaries that commute with the projectors [56, 57]. Considering the Hamiltonian (2.3) in a lattice with open boundary conditions in z-direction, we can define two (quasi-)local symmetry operators, P_j and Q_j. For the top boundary we define the pyramidal and local operators

$$P_j^t \equiv (XXX)_{j+\frac{1}{2}\hat{z}}\, Z_j, \qquad \text{and} \qquad Q_j^t \equiv Z_j, \tag{7.1}$$

where j are the sites of $\tilde{\Lambda}$, as depicted in Fig. 12. Note that P_j^t are localized by sites at $z = L_z - a/2$, while Q_j^t are localized in sites at $z = L_z$, and they corresponds to truncated $\mathcal{O}_p$ of different sublattices. Both operators are symmetries of the Hamiltonian and commute with all TD operators, however note that there are anomalies at boundary, since $\left[P_j^t, Q_j^t\right] \neq 0$. Analogously, it is possible to define P_j^b and Q_j^b at the bottom boundary.

7.1 Anomaly Inflow

Roughly, the idea of anomaly inflow means that an anomaly in the bulk can be related with an anomaly on the boundaries, and the model (2.3) is an enlightening demonstration of this phenomena. Let us define the symmetry operators that extends into

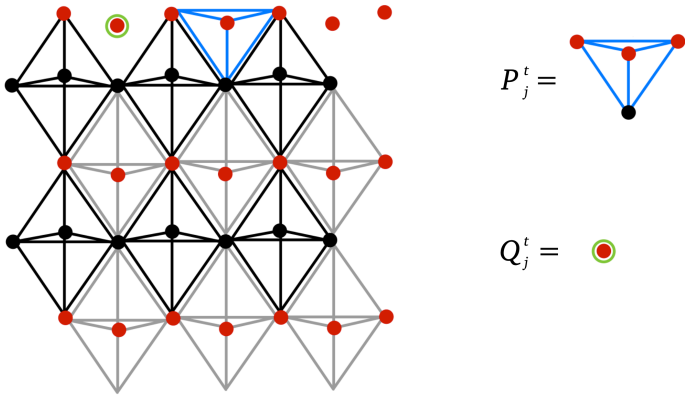

Figure 12 – An top boundary of lattice open in z-direction and the representation of P_j^b and Q_j^b operators.

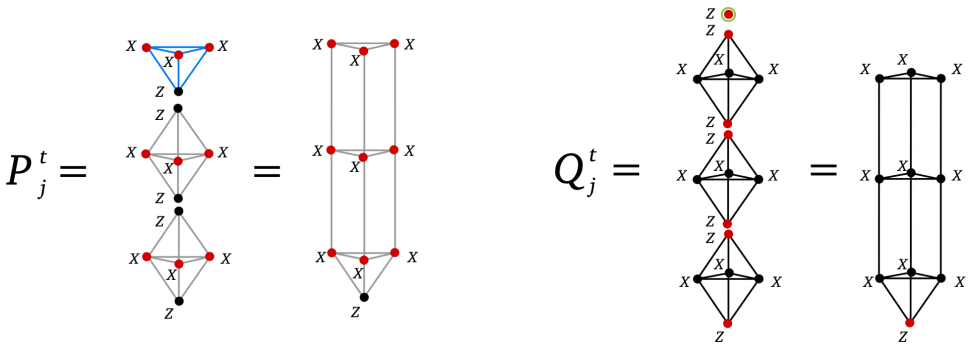

Figure 13 – Representation of $\tilde{P}_j^t$ and $\tilde{Q}_j^t$ operators. They are constructed as products of P_j^t and Q_j^t, respectively, with TD operators.

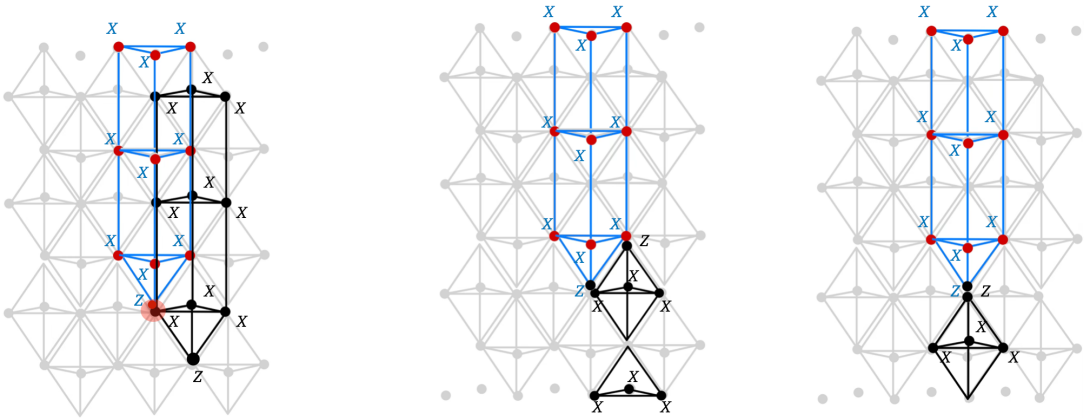

Figure 14 – Representations of $\tilde{P}$ and $\tilde{Q}$ in the bulk. In the first figure, both operators $\tilde{P}$ and $\tilde{Q}$ are attached in the top boundary and the anomaly in the bulk is highlighted. In the last two figures, one operator is attached in the top boundary while the other originates from the bottom boundary, resulting in them not being mutually anomalous.

the bulk,

$$\tilde{P}_i^m(z) \equiv P_i^m \prod_{j \in \mathcal{L}_i^m(z)} \mathcal{O}_j \qquad \text{and} \qquad \tilde{Q}_i^m(z) \equiv Q_i^m \prod_{j \in \mathcal{L}_i^m(z)} \mathcal{O}_j, \tag{7.2}$$

where $m = t$ or b and $\mathcal{L}_i^m(z)$ is a straight line from the m boundary to the point z. Both operators results in kind of tube that shrink to a point in the bulk, as illustrated in Fig. 13.

In terms of P_j^m and Q_j^m, the anomalies are located at the boundaries, however in terms of $\tilde{P}_j^m$ and $\tilde{Q}_j^m$ they are equivalently realized by operators that extends into the bulk. It worth to emphasize that $\tilde{P}$ and $\tilde{Q}$ preserves the commutation relations of P and Q, therefore

$$\left[\tilde{P}_j^t, \tilde{P}_j^b\right] = \left[\tilde{Q}_j^t, \tilde{Q}_j^b\right] = \left[\tilde{P}_j^t, \tilde{Q}_j^b\right] = 0. \tag{7.3}$$

It means that the anomalies of top boundary does not mix with the bottom anomalies, as depicted in Fig. 14.

7.1.1 Anomaly Inflow in Non-Degenerated System Sizes

To make this even more evident, let us consider a non degenerated size L, so that the bulk is anomalous free and all anomalies come from the boundaries. In these cases, it is possible to define

$$B_i^m \equiv \prod_{j \in \tilde{\mathcal{M}}_i^a} P_j^m. \tag{7.4}$$

As discussed in Eq. (4.1), this product results in an isolated X_j and then we can define a one-to-one commutation rule,

$$B_i^m Q_j^n = (-1)^{\delta_{m,n}\delta_{i,j}} Q_j^n B_i^m. \tag{7.5}$$

Therefore, the set of operators $\{B_i^m, Q_i^m\}$ comprehend the $2L^2$ pairs of anomalous symmetry operators.

Following Eq. (7.2), we can define the extended operators

$$\tilde{B}_i^m \equiv B_i^m \prod_{j \in \mathcal{L}_i^m(z)} \prod_{j \in \tilde{\mathcal{M}}_i^a} \mathcal{O}_j, \tag{7.6}$$

with the commutation rules for anomalies in the bulk,

$$\tilde{B}_i^m \tilde{Q}_j^n = (-1)^{\delta_{m,n}\delta_{i,j}} \tilde{Q}_j^n \tilde{B}_i^m. \tag{7.7}$$

In these non-degenerated system sizes, this is a demonstration that the anomalies in the bulk can only come from the boundaries.

7.1.2 Anomaly Inflow in Degenerated System Sizes

When considering degenerated system sizes, the t'Hoof anomalies among M_I^a and W_I^a flows from the bulk to the boundary. It occurs because the membranes are equivalently defined in any plane (see Eq. (3.9)), so that we can put it on one boundary. Then, it is possible to express this membrane symmetry as product of the boundary operators,

$$M_I^a = \prod_{i \in \mathcal{M}_I^a} P_i^m \qquad \text{or} \qquad M_I^a = \prod_{i \in \mathcal{M}_I^a} Q_i^m. \tag{7.8}$$

Consequently, there is a correspondence among the anomalies on the bulk and on the boundaries of this topologically ordered phasses.

7.2 Connection with Fractal 2d models

There are some two-dimensional models with similar fractal properties obtained from Eq. (2.3). As the ground state degeneracy depends exclusively on this fractal structure, the spontaneous symmetry breaking model studied in [48, 54] and the SPT of [52]

turn out to have the same degeneracy. It is enlightening to compare the physics of these models making clear the role of third dimension.

The idea behind the connection of theses models is considering a boundaries that condense different types of charge, and then we get an approximated 2d model by removing the bulk (making $L_z < 1$). Depending if both boundaries condense equal or different type of excitations, the resulting model comprehends an SPT or an Spontaneous Symmetry Breaking phase, respectively [58].

Let us consider a degenerated system size L and open boundary conditions in the z-direction, resulting in a 3d lattice $L \times L \times L_z$. Assuming the Hamiltonian (2.3), the symmetries are M_I^a, W_I^a, and the boundary operators P_i^m and Q_i^m. We say that both boundaries are condensate of $\mathcal{O}_j$ excitations because an local X_j creates (and annihilates) a *single* excitation on the boundaries, in contrast with the bulk where it creates pairs. In this case, both top and bottom boundaries condenses $\mathcal{O}_j$ excitations from sublattices 1 and 2. The role of W_I^a in this open system can be understood as creating an excitation in one edge, carrying it across the whole bulk, and annihilating it on the opposite edge.

We can prevent some condensations including P_j^m and Q_j^m terms in the Hamiltonian. In order to keep a sum of commuting projectors, we can only include one type of operator in each boundary, what makes us define

$$H_c = H - \sum_i \left[\alpha P_i^t + (1-\alpha)\, Q_i^t\right] - \sum_j \left[\beta P_j^b + (1-\beta)\, Q_j^b\right], \tag{7.9}$$

where H is the Hamiltonian defined in Eq. (2.3) and α and $\beta = 0$ or 1. Now, the action of a local X_j in the boundaries affect an $\mathcal{O}_j$ and a P_j^m or Q_j^m simultaneously, what makes impossible to remove an excitation from the system.

There are few possibilities of introducing the boundary operators that result in different properties depending on its sublattices, as illustrated in Fig. 15. If the operators introduced on the top and on the boundary belong to different sublattices, the Wilson line is not a symmetry and all M_I^a reduces to a product of the projectors. Conversely, if the operators introduced on the top and on the boundary belong to the same sublattice, namely a, W_I^b and M_I^b ($b \neq a$) are still symmetries.

Moreover, to reach the $\approx$ 2d system we need to remove the bulk, what means that $L_z < 1$ where no $\mathcal{O}_j$ can contribute to the final Hamiltonian. It only occurs when we include Q^t and Q^b or P^t and P^b that belongs to same sublattices (respectively, cases *I* and *IV* of Fig. 15) or including P^t and Q^b or Q^t and P^b that belongs to different sublattices (respectively, cases *II* and *III*). For the remaining possibilities (cases *V*, *VI*, *VII*, and *VIII*) we cannot remove the bulk completely. The approximated 2d systems are represented in Fig. 16.

In the case *I*, after removing the bulk the Hamiltonian resumes to

$$H_c = -\sum_i Z_i, \tag{7.10}$$

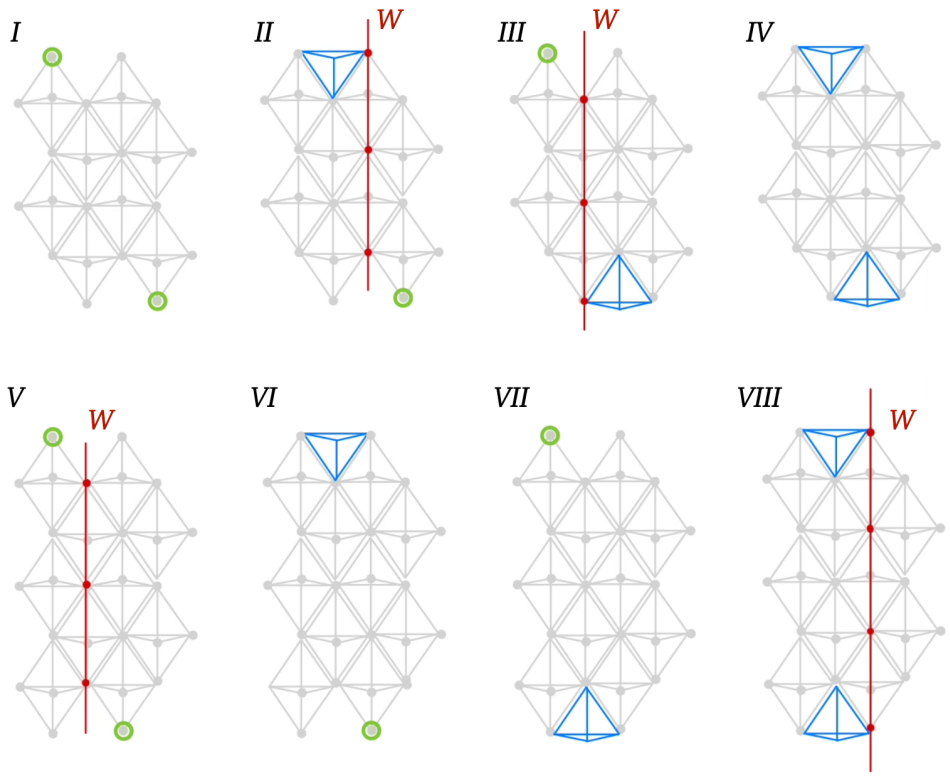

Figure 15 – Representation of different choices of α and β for different lattice structures. The Wilson lines are represented in red only in the cases that the choices allows this symmetry.

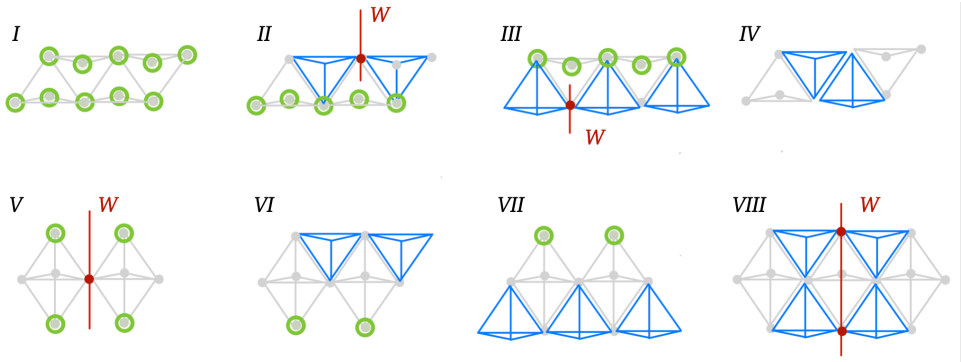

Figure 16 – The resulting systems in ≈ 2d. In the cases V to $VIII$ we verify that $\mathcal{O}$ is still fitting in the lattice.

that describes a paramagnet in a 2d hexagonal lattice (combining both layers in a unique). The first non-trivial situation is the cases II, that results in

$$H_c = -\sum_i P_i^t - \sum_j Q_j^b. \tag{7.11}$$

In this case the Q_i^b operators completely define the eigenstates of its sites and effectively reduces the Hamiltonian to

$$H_c = -\sum_{i,j,k \in \triangle} X_i X_j X_k, \tag{7.12}$$

exactly the triangular plaquette model [48, 54]. In this spontaneous symmetry breaking phase, the Wilson lines reduces to local operators X_j that plays the role of order parameter, while the fractal membranes are analogous to the global symmetry.

By introducing the boundary operators P^t and P^b as depicted in the case IV of Fig. 16, the 2d Hamiltonian results in

$$H_c = \sum_i P_i^t + P_i^b. \tag{7.13}$$

This result recover the Sierpinski fractal Symmetry protected topological phase studied in [52]. In this case the Wilson lines are not symmetries and the membrane operators are trivial, because it reduces to a product of P^t and P^b.

As discussed previously, the model (2.3) is topological ordered because long range entanglement makes impossible to deform into a product state in finite time. The nontrivial mutual statistic depends on the mobility along the z-direction, and the two dimensional models cannot exhibit the long range entanglement. Additionally, in the cases where a two-dimensional fractal model presents nontrivial ground state degeneracy there is a local operator distinguishing different ground states. Consequently, the two-dimensional fractal models are not topologically ordered. This is the reason why they lies out the Haah's bound [59] for ground state degeneracy.

8 Effective Field Theory and Edge Modes

The effective field theory of a system is a description that captures fundamental part of the physics in te low energy limit. Such descriptions are powerful tools for examining various aspects of the system in the presence of boundaries, such as edge modes and the symmetry breaking on the boundaries. It is important to mention that due to the subtleties of the subsystem symmetries and fractal dynamics, we will never take the strict continuous limit.

In the case of model (2.3), a bosonic Hamiltonian on the HPC lattice that captures the dynamics of excitations will preserve the topological properties and certain symmetry aspects in the deep infrared (IR) limit [60]. It is possible to describe the quasi-particle in terms of matter coupled with gauge fields in a Higgs phase. In this context, the deep IR limit corresponds to the energy scales where the excitations above the ground state become inaccessible, and the physics is governed by a BF Lagrangian.

In this system, the allowed processes for quasi-particle creation involves transitions from the vacuum to two and three excitations, implemented by the X_i and Z_i operators, respectively. A local X_i operator allows the creation or annihilation of excitations along the $\hat{z}$ axis, while a Z_i operator allows it for three excitations arranged in a triangular configuration on the xy plane. A bosonic theory with kinetic terms capable to reproduce this pattern is given by the Hamiltonian

$$H = -J \sum_{\vec{r}} b_{\vec{r}}\, b_{\vec{r}+\vec{e}_1}\, b_{\vec{r}+\vec{e}_2} + \rho_0\, {b_{\vec{r}}}^{\dagger}\, b_{\vec{r}+\hat{z}} + \text{h.c.} + \dots \ , \tag{8.1}$$

where $\vec{e}_i$ represents lattice vectors and ρ_0 is a dimensional parameter. This effective Hamiltonian can be expressed in a gauge invariant form by introducing Higgs fields, $b_{\vec{r}} = \rho_{\vec{r}} e^{i\phi_{\vec{r}}}$. In the broken symmetry phase, this field acquires a vacuum expected value, $\langle \rho_{\vec{r}} \rangle = \rho_0$, and the slow changes of the $\phi_{\vec{r}}$ are captured by

$$H = \sum_{\vec{r}} \frac{\tilde{J}}{2} \left(\Delta_{xy} \phi_{\vec{r}}\right)^2 + \frac{\tilde{J}}{2} \left(\Delta_z \phi_{\vec{r}}\right)^2 + \frac{g}{2} \Pi_{\vec{r}}^2 \tag{8.2}$$

where $\Pi_{\vec{r}}$ and $\phi_{\vec{r}}$ are canonically conjugated, $[\phi_{\vec{r}}, \Pi_{\vec{r}'}] = i\delta_{r,r'}$, and we introduced the lattice operators that act as

$$\Delta_{xy}\, f_{\vec{r}} = \frac{f_{\vec{r}} + f_{\vec{r}+\vec{e}_1} + f_{\vec{r}+\vec{e}_2}}{a} \qquad \text{and} \qquad \Delta_z\, f_{\vec{r}} = \frac{f_{\vec{r}+\hat{z}} - f_{\vec{r}}}{a}. \tag{8.3}$$

It's important to note that the theory is only invariant under shifts $\phi \to \phi + \alpha$ for a function α dependent of the coordinates if it is annihilated by Δ_{xy} and Δ_z.

The gauge fields can be implemented through the minimal coupling with the matter field,

$$H = \sum_{\vec{r}} \frac{\tilde{J}}{2} \left(\Delta_{xy}\phi - \frac{q}{a} A_{xy}\right)^2 + \frac{\tilde{J}}{2} \left(\Delta_z \phi - \frac{q}{a} A_z\right)^2 + \frac{g}{2} \Pi^2 + \frac{h_{xy}}{2} E_{xy}^2 + \frac{h_z}{2} E_z^2, \tag{8.4}$$

and the dynamics is introduced with the canonical conjugated momenta E_k^a, respecting the commutation relation $[A_k(r), E_{k'}(r')] = i\delta_{k,k'}\delta_{r,r'}$, where $k = xy, z$. This formulation is invariant under local gauge transformations

$$\phi \to \phi + qf(r), \quad \text{and} \quad A_k \to A_k + \Delta_k f(r). \tag{8.5}$$

At this point, ϕ has a general charge q under the gauge transformation.

Using the canonical commutation relations, it is possible to check that there is a conserved quantity associated with the momenta E_k and Π,

$$\left[\Delta'_{xy}E_{xy} - \Delta_z E_z + \frac{q}{a}\Pi, H\right] = 0, \tag{8.6}$$

where Δ'_k corresponds to

$$\Delta'_{xy} f_{\vec{r}} = \frac{f_{\vec{r}} + f_{\vec{r}-\vec{e}_1} + f_{\vec{r}-\vec{e}_2}}{a}. \tag{8.7}$$

Notice that under PBC, it holds the identity

$$\begin{aligned}\sum_{\vec{r}} f_{\vec{r}}\,\Delta_{xy} g_{\vec{r}} &= \sum_{\vec{r}} f_r\left(g_{\vec{r}} + g_{\vec{r}+\vec{e}_1} + g_{\vec{r}+\vec{e}_2}\right)\\ &= \sum_{\vec{r}} g_r\left(f_{\vec{r}} + f_{\vec{r}-\vec{e}_1} + f_{\vec{r}-\vec{e}_2}\right)\\ &= \sum_{\vec{r}} g_{\vec{r}}\,\Delta'_{xy} f_{\vec{r}}.\end{aligned} \tag{8.8}$$

The conservation (8.6) is analogous to a Gauss law in presence of matter and can be enforced energetically with a Lagrange multiplier field A_t,

$$\begin{aligned}H = \sum_{\vec{r}} &\frac{\tilde{J}}{2}\left(\Delta_{xy}\phi - \frac{q}{a}A_{xy}\right)^2 + \frac{\tilde{J}}{2}\left(\Delta_z\phi - \frac{q}{a}A_z\right)^2 + \frac{g}{2}\Pi^2 + \frac{h_{xy}}{2}E_{xy}^2 + \frac{h_z}{2}E_z^2,\\ &- A_t\left(\Delta'_{xy}E_{xy} - \Delta_z E_z + \frac{q}{a}\Pi\right).\end{aligned} \tag{8.9}$$

It is interesting to observe that a term $\left(\Delta_z A_{xy} - \Delta'_{xy}A_z\right)^2$, analogous to magnetic field in $2+1$ d, is compatible with the gauge invariance (8.5) and could be introduced in this Hamiltonian. However, it will be neglect because it does not contribute at the energy scales that we are interested in.

The conjugated momenta E_k^a and Π^a can be found explicitly using the Hamilton equation,

$$\Pi = \frac{a\,\partial_t\phi - qA_t}{a\,g}, \quad E_{xy} = \frac{\partial_t A_{xy} - \Delta_{xy}A_t}{h_{xy}} \quad \text{and} \quad E_z = \frac{\partial_t A_z - \Delta_z A_t}{h_z} \tag{8.10}$$

and by a Legendre transformation we find the Lagrangian

$$\begin{aligned}L = \sum_{\vec{r}} &\frac{g'}{2}\left(qA_t - a\partial_t\phi\right)^2 + \frac{1}{2h_{xy}}\left(\Delta_{xy}A_t - \partial_t A_{xy}\right)^2 + \frac{1}{2h_z}\left(\Delta_z A_t - \partial_t A_z\right)^2\\ &- \frac{\tilde{J}}{2}\left(qA_{xy} - a\Delta_{xy}\phi\right)^2 - \frac{\tilde{J}}{2}\left(qA_z - a\Delta_z\phi\right)^2,\end{aligned} \tag{8.11}$$

where we redefine $g\,a^2 = 1/g'$ and keep the massive parameters $\left[\tilde{J}\right] = [h] = [g'] = 1$. With this Lagrangian, it is possible to implement fields dual to ϕ in order to find a pure gauge representation. Defining $C_t \equiv a\partial_t\phi$ and $C_k \equiv a\,\Delta_k\phi$, we get

$$\begin{aligned} L = \sum_{\vec{r}} & \frac{g'}{2}\left(qA_t - C_t\right)^2 + \frac{1}{2h_{xy}}\left(\Delta_{xy}A_t - \partial_t A_{xy}\right)^2 + \frac{1}{2h_z}\left(\Delta_z A_t - \partial_t A_z\right)^2 \\ & - \frac{\tilde{J}}{2}\left(qA_{xy} - C_{xy}\right)^2 - \frac{\tilde{J}}{2}\left(qA_z - C_z\right)^2 \\ & + \frac{1}{2\pi}\left[B_t\left(\Delta'_{xy}C_z - \Delta'_z C_{xy}\right) + B_{xy}\left(\Delta_z C_t - \partial_t C_z\right) - B_z\left(\Delta_{xy}C_t - \partial_t C_{xy}\right)\right] \end{aligned} \tag{8.12}$$

The last terms was introduced to enforce dynamically the constraints $\Delta_k C_t = \partial_t C_k$ and $\Delta_{xy}C_z = \Delta_z C_{xy}$. Integrating out the field C results in a pure gauge Lagrangian in terms of A and B fields,

$$\begin{aligned} L = \sum_{\vec{r}} & -\frac{1}{8\pi^2 g'}\left(\Delta_z B_{xy} - \Delta'_{xy}B_z\right)^2 + \frac{1}{2h_{xy}}\left(\partial_t A_{xy} - \Delta_{xy}A_t\right)^2 + \frac{1}{2h_z}\left(\partial_t A_z - \Delta_z A_t\right)^2 \\ & + \frac{1}{8\pi^2\tilde{J}}\left(\partial_t B_{xy} + \Delta'_{xy}B_t\right)^2 + \frac{1}{8\pi^2\tilde{J}}\left(\partial_t B_z + \Delta_z B_t\right)^2 \\ & + \frac{q}{2\pi}\left[B_t\left(\Delta_{xy}A_z - \Delta_z A_{xy}\right) + B_{xy}\left(\Delta_z A_t - \partial_t A_z\right) + B_z\left(\partial_t A_{xy} - \Delta_{xy}A_t\right)\right]. \end{aligned} \tag{8.13}$$

The ground state properties become manifestly relevant in the deep infrared limit, where all gapped excitation become inaccessible to the system. This energy scales corresponds to take $\tilde{J}, g', h_{xy}, h_z \to \infty$, and results in a system dominated by a BF theory, remaining only the symmetries and topological properties of ground state,

$$L = \sum_{\vec{r}} \frac{q}{2\pi}\left[B_t\left(\Delta_{xy}A_z - \Delta_z A_{xy}\right) + B_{xy}\left(\Delta_z A_t - \partial_t A_z\right) + B_z\left(\partial_t A_{xy} - \Delta_{xy}A_t\right)\right]. \tag{8.14}$$

From the several forms that the action of the theory (8.14) can be written, let us consider

$$S = \int dt \sum_{xy}\sum_{z} \frac{1}{\pi}\left[B_t\left(\Delta_{xy}A_z - \Delta_z A_{xy}\right) - A_t\left(\Delta_z B_{xy} + \Delta'_{xy}B_z\right) + B_z\partial_t A_{xy} - B_{xy}\partial_t A_z\right], \tag{8.15}$$

in which becomes evident the gauge invariance under

$$A_t \to A_t + \partial_t f, \qquad A_{xy} \to A_{xy} + \Delta_{xy}f, \qquad A_z \to A_z + \Delta_z f, \tag{8.16}$$

$$B_t \to B_t + \partial_t g, \qquad B_{xy} \to B_{xy} - \Delta'_{xy}g, \qquad B_z \to B_z + \Delta_z g. \tag{8.17}$$

On periodic manifolds, it is possible to define gauge invariant quantities, given by the extended objects

$$W_A(\gamma_I) = \exp\left(i\,q_e \sum_{\hat{z}\in\gamma_I} A_z\right), \quad \text{and} \quad W_B(\gamma_I) = \exp\left(i\,q_m \sum_{\hat{z}\in\gamma_I} B_z\right), \tag{8.18}$$

defined on closed lines γ_I along z direction, and

$$T_A(M_I) = \exp\left(i\,q_e \sum_{\vec{r}\in M_I} A_{xy}\right), \quad \text{and} \quad T_B(M_I) = \exp\left(i\,q_m \sum_{\vec{r}\in M_I} B_{xy}\right), \tag{8.19}$$

on M_I is a closed fractal membranes on xy directions. These non-trivial gauge invariant objects are analogous to the Wilson lines and t' Hooft membranes constructed on the exact theory. To satisfy the compactness of the fields, the parameter q_e and q_m must be integers. For example, the condition $A_z \sim A_z + \frac{2\pi}{L_z}$ implies that q_e is an integer, and similarly for A_{xy}, B_z and B_{xy}.

Considering the Lagrangian (8.11), the canonical momentum is given by

$$E_{xy} = \frac{\partial L}{\partial\left(\partial_t A_{xy}\right)} = \frac{q}{2\pi} B_z \quad \text{and} \quad E_z = \frac{\partial L}{\partial\left(\partial_t A_z\right)} = -\frac{q}{2\pi} B_{xy}, \tag{8.20}$$

therefore the fields A_k and B_k are canonically conjugated to each other

$$\left[A_k(r), B_l(r')\right] = \frac{2\pi i}{q} \epsilon^{lk} \delta_{rr'}. \tag{8.21}$$

As a consequence, the algebra among Wilson lines and t' Hooft membranes are

$$W_A\left(\gamma_I\right) T_B\left(M_J\right) = e^{-\frac{2\pi i\, q_e q_m}{q} \delta_{IJ}} T_B\left(M_J\right) W_A\left(\gamma_I\right), \tag{8.22}$$

and analogously to W_B and T_A. There are some operators that induces the same holonomies and can be identified as the same, $q_e \sim q_e + q$ and $q_m \sim q_m + q$. The nontrivial commutation of the gauge operators suggests that the Higgs phase spontaneously break the $U(1)$ symmetry down to $\mathbb{Z}_q$ and gaps out the gauge fields. In order to recover the $\mathbb{Z}_2$ algebra we can set the charge $q = 2$ and them q_e and q_m are constrained to be $q_e = q_m = 1$.

Introducing physical boundaries on the system described by the Lagrangian (8.11), it is possible to understand the edge modes from the perspective of an effective field description. Suppose we place the theory (8.15) on a manifold periodic in x and y directions but with an open boundary boundaries in z direction, at $z = 0$. Under these conditions, the bulk action is no longer invariant under the gauge transformation (8.16) and (8.17), but changes by a boundary terms,

$$\begin{aligned} S_{\text{Bulk}} &= \frac{1}{\pi} \int dt \sum_{xy} \sum_{z=-\infty}^{0} \partial_t g\left(\Delta_{xy} A_z - \Delta_z A_{xy}\right) - \partial_t f\left(\Delta_z B_{xy} + \Delta'_{xy} B_z\right) \\ &\quad + \Delta_z g\, \partial_t\left(A_{xy} + \Delta_{xy} f\right) + \Delta'_{xy} g\, \partial_t\left(A_z + \Delta_z f\right) + B_z\, \partial_t \Delta_{xy} f - B_{xy}\, \partial_t \Delta_z f \\ &= \frac{1}{\pi} \int dt \sum_{xy} \sum_{z=-\infty}^{0} \Delta_z\left(g\, \partial_t A_{xy} + f\, \partial_t B_{xy} - \partial_t g\, \Delta_{xy} f\right) \\ &= \frac{1}{\pi} \int dt \sum_{xy} g\, \partial_t A_{xy} + f\, \partial_t B_{xy} - \partial_t g\, \Delta_{xy} f \Big|_{z=0}. \end{aligned} \tag{8.23}$$

This implies that gauge degrees of freedom become physical degrees of freedom at the edge. The action of the complete system, given by

$$S = S_{\text{Bulk}} + S_{\text{Edge}} \tag{8.24}$$

is still invariant under the gauge transformations, which allows us to infer

$$S_{\text{Edge}} = \frac{1}{2\pi} \int dt \sum_{xy} \theta\left(\Delta_{xy} A_t - \partial_t A_{xy}\right) - \varphi\left(\partial_t B_{xy} + \Delta'_{xy} B_t\right) + \left(A_{xy} B_t - A_t B_{xy}\right). \tag{8.25}$$

In this setup we can check that S is invariant under (8.16) and (8.17) combined with the boundary transformations $\varphi \to \varphi + f$ and $\theta \to \theta + g$.

The the equation of motion of S_{Edge} are solved by

$$A_t = a\,\partial_t\varphi, \qquad A_{xy} = a\,\Delta_{xy}\varphi, \qquad B_t = -a\,\partial_t\theta \qquad B_{xy} = a\,\Delta'_{xy}\theta, \tag{8.26}$$

that reduces the action to

$$S_{\text{Edge}} = \frac{a}{\pi}\int dt \sum_{xy} \partial_t\theta\,\Delta_{xy}\varphi. \tag{8.27}$$

In this scenario, the canonical conjugated momentum is

$$\frac{\delta L}{\delta\,\partial_t\theta} = \frac{a}{\pi}\Delta_{xy}\varphi \qquad \text{and} \qquad \frac{\delta L}{\delta\,\partial_t\varphi} = \frac{a}{\pi}\Delta'_{xy}\theta, \tag{8.28}$$

and the commutation relations become

$$\left[\varphi(r), \Delta'_{xy}\theta(r')\right] = i\frac{\pi}{a}\delta_{r,r'} \qquad \text{and} \qquad \left[\theta(r), \Delta_{xy}\varphi(r')\right] = -i\frac{\pi}{a}\delta_{r,r'}. \tag{8.29}$$

Applying the solution of the equation of motion (8.26) to the gauge invariant operators reduce the Wilson lines to local operators at the boundary,

$$W_A = e^{i\,\varphi_{z=0}}, \quad \text{and} \quad W_B(\gamma_I) = e^{i\,\theta_{z=0}}, \tag{8.30}$$

and the t' Hooft membrane operators become

$$T_A = \exp\left(i\,a\sum_{\vec{r}\in M'_I}\Delta_{xy}\varphi\right), \quad \text{and} \quad T_B = \exp\left(i\,a\sum_{\vec{r}\in M_I}\Delta'_{xy}\theta\right). \tag{8.31}$$

Therefore, at the boundary the symmetry operators acts on the fields as

$$T_A{}^\dagger\,\theta\,T_A = \theta + \pi \quad \text{and} \quad T_B{}^\dagger\,\varphi\,T_B = \varphi + \pi. \tag{8.32}$$

The boundary exhibits fluctuation of the two scalar fields, φ and θ, with fractal dynamics. The perturbations invariant under $\theta \to \theta + \pi$ and $\varphi \to \varphi + \pi$ do not break the symmetry explicitly. In the action, it equivalent to perturb as

$$S_{\text{Edge}} = \int dt \sum_{xy} \frac{1}{\pi}\partial_t\theta\,\Delta_{xy}\varphi + K_1\left(\Delta_{xy}\varphi\right)^2 + K_2\left(\Delta_{xy}\theta\right)^2 + \lambda_1\cos\left(2\varphi\right) + \lambda_2\cos\left(2\theta\right). \tag{8.33}$$

The terms $\cos(2\varphi)$ and $\cos(2\theta)$, even preserving the $\mathbb{Z}_2$ symmetry, they lead to a spontaneous symmetry breaking by pinning the fluctuation. Consider, for example, the term $\cos\left(2\varphi\right)$ fixing the value of φ to 0 or π. These values make the operator $\cos\left(\varphi\right)$ to acquire a vacuum expected value. It is odd by the symmetry $\varphi \to \varphi + \pi$ and plays the role of order parameter. In the meantime, pinning the value of φ implies that W_A and T_A are also pinned. The relation (8.22) indicates that if $\langle W_A\rangle \neq 0$ and $\langle T_A\rangle \neq 0$, (or, in other words, Higgsing A_{xy} and A_z,) infers that the gauge potential B_{xy} and B_z is strongly fluctuating. In other words, while a field is pinned, its conjugated is strongly fluctuating, and both cannot be pinned simultaneously, consequently the symmetries cannot be spontaneously broken at same time. Thus, there is no way to gap out the gapless modes at the surface due to the subsystem symmetries.

9 Conclusions

We have reported on a model that presents exotic topological order due to an intricate interplay between fractal subsystem symmetries and the lattice size. The fractal subsystem symmetries are quite sensitive to the lattice size and exist only for system sizes $L_x \times L_y$ of the form $L_x = k\left(2^n - 2^m\right)$ and $L_y = L_x/r$, with integers $k \geq 1$, $r \geq 1$, $n > 2$, and $m \geq 0$, satisfying $n > m+1$. The fractal symmetries possess mixed 't Hooft anomalies with the line subsystem symmetries, which lead to a nontrivial ground state degeneracy. This amounts to the spontaneous breaking of the fractal symmetry. For the remaining sizes, the fractal symmetry is explicitly broken and there are no fractal membrane operators that commute with the Hamiltonian. Consequently, there are no mixed 't Hooft anomalies and the ground state is unique. Despite the unique global anyonic superselection sector, such cases are topologically ordered, since the ground state is still long-range entangled.

We have also described the physics of these phases in a manifold with boundaries. The truncated stabilizer operators at the edge can be connected with symmetries that extend into the bulk, which enlightens our understanding of anomaly inflow. By considering only the boundary physics, we can connect this phase either with an SPT phase or an SSB phase, depending on whether the boundaries condense different or the same type of excitations, respectively. With the effective theory, we demonstrate that the mutually anomalous symmetries at the boundary cannot be simultaneously broken at same time.

References

1 WEN, X.-G. Colloquium: Zoo of quantum-topological phases of matter. **Reviews of Modern Physics**, American Physical Society (APS), v. 89, n. 4, dez. 2017. Cited on page 1.

2 CHAMON, C. Quantum glassiness in strongly correlated clean systems: An example of topological overprotection. **Physical Review Letters**, American Physical Society (APS), v. 94, n. 4, jan. 2005. ISSN 1079-7114. Cited on page 1.

3 BRAVYI, S.; LEEMHUIS, B.; TERHAL, B. M. Topological order in an exactly solvable 3d spin model. **Annals of Physics**, Elsevier BV, v. 326, n. 4, p. 839–866, abr. 2011. ISSN 0003-4916. Cited 2 times on page 1 and 2.

4 HAAH, J. Local stabilizer codes in three dimensions without string logical operators. **Physical Review A**, American Physical Society (APS), v. 83, n. 4, abr. 2011. ISSN 1094-1622. Cited 2 times on page 1 and 2.

5 VIJAY, S.; HAAH, J.; FU, L. A new kind of topological quantum order: A dimensional hierarchy of quasiparticles built from stationary excitations. **Physical Review B**, American Physical Society (APS), v. 92, n. 23, p. 235136, dez. 2015. Cited on page 1.

6 PREM, A.; HAAH, J.; NANDKISHORE, R. Glassy quantum dynamics in translation invariant fracton models. **Physical Review B**, American Physical Society (APS), v. 95, n. 15, abr. 2017. Cited on page 1.

7 SLAGLE, K.; KIM, Y. B. Quantum field theory of x-cube fracton topological order and robust degeneracy from geometry. **Physical Review B**, American Physical Society (APS), v. 96, n. 19, nov. 2017. Cited on page 1.

8 YOU, Y. et al. Symmetric fracton matter: Twisted and enriched. Elsevier BV, v. 416, p. 168140, maio 2020. Cited on page 1.

9 SHIRLEY, W.; SLAGLE, K.; CHEN, X. Universal entanglement signatures of foliated fracton phases. **SciPost Physics**, Stichting SciPost, v. 6, n. 1, jan. 2019. Cited on page 1.

10 SHIRLEY, W.; SLAGLE, K.; CHEN, X. Twisted foliated fracton phases. **Physical Review B**, American Physical Society (APS), v. 102, n. 11, set. 2020. ISSN 2469-9969. Cited on page 1.

11 FUJI, Y. Anisotropic layer construction of anisotropic fracton models. **Physical Review B**, American Physical Society (APS), v. 100, n. 23, dez. 2019. Cited on page 1.

12 FONTANA, W.; GOMES, P.; CHAMON, C. Lattice clifford fractons and their chern-simons-like theory. **SciPost Physics Core**, Stichting SciPost, v. 4, n. 2, p. 012, maio 2021. Cited 2 times on page 1 and 2.

13 FONTANA, W.; GOMES, P.; CHAMON, C. Field theories for type-II fractons. **SciPost Physics**, Stichting SciPost, v. 12, n. 2, p. 064, fev. 2022. Cited on page 1.

14 NANDKISHORE, R. M.; HERMELE, M. Fractons. **Annual Review of Condensed Matter Physics**, Annual Reviews, v. 10, n. 1, p. 295–313, mar. 2019. Cited on page 1.

15 PRETKO, M.; CHEN, X.; YOU, Y. Fracton phases of matter. World Scientific Pub Co Pte Lt, v. 35, n. 06, p. 2030003, fev. 2020. Cited on page 1.

16 VIJAY, S.; HAAH, J.; FU, L. Fracton topological order, generalized lattice gauge theory and duality. **Physical Review B**, American Physical Society (APS), v. 94, n. 23, dez. 2016. Cited 2 times on page 1 and 2.

17 PRETKO, M. Subdimensional particle structure of higher rank $u(1)$ spin liquids. **Physical Review B**, American Physical Society (APS), v. 95, n. 11, mar. 2017. ISSN 2469-9969. Cited on page 1.

18 JANGJAN, M.; HOSSEINI, M. V. Topological properties of subsystem-symmetry-protected edge states in an extended quasi-one-dimensional dimerized lattice. **Physical Review B**, American Physical Society (APS), v. 106, n. 20, nov. 2022. Cited on page 1.

19 DELFINO, G.; YOU, Y. Anyon condensation web and multipartite entanglement in 2d fracton-like theories. arXiv, out. 2023. Cited on page 1.

20 GAIOTTO, D. et al. Generalized global symmetries. Springer Science and Business Media LLC, v. 2015, n. 2, p. 172, fev. 2015. Cited on page 1.

21 GOMES, P. R. S. An introduction to higher-form symmetries. **SciPost Physics Lecture Notes**, Stichting SciPost, v. 74, set. 2023. Cited on page 1.

22 BRENNAN, T. D.; HONG, S. Introduction to generalized global symmetries in qft and particle physics. arXiv, jun. 2023. Cited on page 1.

23 LUO, R.; WANG, Q.-R.; WANG, Y.-N. Lecture notes on generalized symmetries and applications. arXiv, jul. 2023. Cited on page 1.

24 BHARDWAJ, L. et al. Lectures on generalized symmetries. arXiv, jul. 2023. Cited on page 1.

25 WEN, X.-G. Emergent anomalous higher symmetries from topological order and from dynamical electromagnetic field in condensed matter systems. **Physical Review B**, American Physical Society (APS), v. 99, n. 20, maio 2019. ISSN 2469-9969. Cited on page 1.

26 QI, M.; RADZIHOVSKY, L.; HERMELE, M. Fracton phases via exotic higher-form symmetry-breaking. **Annals of Physics**, Elsevier BV, v. 424, p. 168360, jan. 2021. Cited on page 1.

27 RAYHAUN, B. C.; WILLIAMSON, D. J. Higher-form subsystem symmetry breaking: Subdimensional criticality and fracton phase transitions. Stichting SciPost, v. 15, n. 1, jul. 2023. Cited on page 1.

28 BONDERSON, P.; NAYAK, C. Quasi-topological phases of matter and topological protection. **Physical Review B**, American Physical Society (APS), v. 87, n. 19, maio 2013. ISSN 1550-235X. Cited on page 1.

29 HUXFORD, J.; NGUYEN, D. X.; KIM, Y. B. Gaining insights on anyon condensation and 1-form symmetry breaking across a topological phase transition in a deformed toric code model. arXiv, maio 2023. Cited on page 1.

30 MCGREEVY, J. Generalized symmetries in condensed matter. Annual Reviews, v. 14, n. 1, p. 57–82, mar. 2023. ISSN 1947-5462. Cited on page 1.

31 PACE, S. D.; WEN, X.-G. Exact emergent higher-form symmetries in bosonic lattice models. **Physical Review B**, American Physical Society (APS), v. 108, n. 19, nov. 2023. ISSN 2469-9969. Cited on page 1.

32 CHERMAN, A.; JACOBSON, T. Emergent 1-form symmetries. arXiv. Cited on page 1.

33 FRÖHLICH, J. et al. Kramers-wannier duality from conformal defects. **Physical Review Letters**, American Physical Society (APS), v. 93, n. 7, ago. 2004. ISSN 1079-7114. Cited on page 1.

34 FRÖHLICH, J. et al. Defect lines, dualities, and generalised orbifolds. In: _____. **XVIth International Congress on Mathematical Physics**. [S.l.]: WORLD SCIENTIFIC, 2010. p. 608–613. ISBN 981430462X. Cited on page 1.

35 CHANG, C.-M. et al. Topological defect lines and renormalization group flows in two dimensions. Springer Science and Business Media LLC, v. 2019, n. 1, jan. 2019. ISSN 1029-8479. Cited on page 1.

36 SCHAFER-NAMEKI, S. Ictp lectures on (non-)invertible generalized symmetries. Elsevier BV, v. 1063, p. 1–55, abr. 2024. ISSN 0370-1573. Disponível em: <https://www.sciencedirect.com/science/article/pii/S0370157324000310>. Cited on page 1.

37 SHAO, S.-H. What's done cannot be undone: Tasi lectures on non-invertible symmetry. arXiv. Cited on page 1.

38 HOOFT, G. 't. Naturalness, chiral symmetry, and spontaneous chiral symmetry breaking. In: _____. **Recent Developments in Gauge Theories**. [S.l.]: Springer US. (NATO Science Series B:, v. 59), p. 135–157. ISBN 978-1-4684-7571-5. Cited on page 1.

39 ZHOU, Z. et al. Fractal quantum phase transitions: Critical phenomena beyond renormalization. arXiv, maio 2021. Cited on page 2.

40 SEIBERG, N.; SHAO, S.-H. Exotic $u(1)$ symmetries, duality, and fractons in 3+1-dimensional quantum field theory. **SciPost Physics**, Stichting SciPost, v. 9, n. 4, out. 2020. ISSN 2542-4653. Cited on page 2.

41 YOU, Y. et al. Fractonic chern-simons and bf theories. **Physical Review Research**, American Physical Society (APS), v. 2, n. 2, maio 2020. ISSN 2643-1564. Cited on page 2.

42 LAKE, E. Renormalization group and stability in the exciton bose liquid. American Physical Society (APS), v. 105, n. 7, fev. 2022. ISSN 2469-9969. Cited on page 2.

43 OH, Y.-T. et al. Rank-2 toric code in two dimensions. American Physical Society (APS), v. 105, n. 4, jan. 2022. ISSN 2469-9969. Cited on page 2.

44 PACE, S. D.; WEN, X.-G. Position-dependent excitations and uv/ir mixing in the $\mathbb{Z}_N$ rank-2 toric code and its low-energy effective field theory. **Physical Review B**, American Physical Society (APS), v. 106, n. 4, jul. 2022. ISSN 2469-9969. Cited on page 2.

45 DELFINO, G. et al. Effective fractonic behavior in a two-dimensional exactly solvable spin liquid. **SciPost Physics**, Stichting SciPost, v. 14, n. 1, jan. 2023. ISSN 2542-4653. Cited on page 2.

46 WATANABE, H.; CHENG, M.; FUJI, Y. Ground state degeneracy on torus in a family of $\mathbb{Z}_n$ toric code. **Journal of Mathematical Physics**, AIP Publishing, v. 64, n. 5, maio 2023. ISSN 1089-7658. Cited on page 2.

47 MA, H. et al. Fracton topological order via coupled layers. **Physical Review B**, American Physical Society (APS), v. 95, n. 24, jun. 2017. ISSN 2469-9969. Cited on page 2.

48 NEWMAN, M. E. J.; MOORE, C. Glassy dynamics and aging in an exactly solvable spin model. **Physical Review E**, American Physical Society (APS), v. 60, n. 5, p. 5068–5072, nov. 1999. ISSN 1095-3787. Cited 3 times on page 2, 23, and 26.

49 CASTELNOVO, C.; CHAMON, C. Topological quantum glassiness. **Philosophical Magazine**, Informa UK Limited, v. 92, n. 1–3, p. 304–323, jan. 2012. ISSN 1478-6443. Cited 2 times on page 2 and 3.

50 YOSHIDA, B. Exotic topological order in fractal spin liquids. **Physical Review B**, American Physical Society (APS), v. 88, n. 12, p. 125122, set. 2013. Cited on page 2.

51 BULMASH, D.; BARKESHLI, M. Generalized $u(1)$ gauge field theories and fractal dynamics. arXiv, jun. 2018. Cited on page 2.

52 DEVAKUL, T. et al. Fractal symmetric phases of matter. **SciPost Physics**, Stichting SciPost, v. 6, n. 1, jan. 2019. Cited 4 times on page 2, 5, 23, and 26.

53 MYERSON-JAIN, N. E. et al. Pascal's triangle fractal symmetries. **Physical Review Letters**, American Physical Society (APS), v. 128, n. 11, mar. 2022. ISSN 1079-7114. Cited on page 2.

54 SFAIROPOULOS, K. et al. Boundary conditions dependence of the phase transition in the quantum newman-moore model. American Physical Society (APS), v. 108, n. 17, nov. 2023. ISSN 2469-9969. Cited 3 times on page 2, 23, and 26.

55 CASASOLA, H. et al. Fractal subsystem symmetries, 't hooft anomalies, and uv/ir mixing. arXiv, out. 2023. Cited 3 times on page 2, 3, and 4.

56 FONTANA, W. B.; PEREIRA, R. G. Boundary modes in the chamon model. **SciPost Physics**, Stichting SciPost, v. 15, n. 1, p. 10, jul. 2023. ISSN 2542-4653. Cited on page 21.

57 SCHUSTER, T. et al. A holographic view of topological stabilizer codes. arXiv, p. 29, dez. 2023. Cited on page 21.

58 ZHANG, C.; CÓRDOVA, C. Anomalies of $(1+1)d$ categorical symmetries. arXiv, p. arXiv:2304.01262, abr. 2023. Cited on page 24.

59 HAAH, J. A degeneracy bound for homogeneous topological order. **SciPost Physics**, Stichting SciPost, v. 10, n. 1, jan. 2021. Cited on page 26.

60 GUO, C.-X. et al. Non-hermitian dynamic strings and anomalous topological degeneracy on a non-hermitian toric-code model with parity-time symmetry. American Physical Society, v. 101, p. 144439. ISSN 2469-9969. Cited on page 27.

Appendix

A Fractal Configurations

The configurations given by Eq. (2.21) behave as basis elements of the set of first lines, $\{S_1(x)\}$, in the sense that it forms a Module (a generalization of the notion of a vector space for fields defined in a ring[1]). As discussed in Sec. 2.1, for a size $L = 2^n - 2^m$ there are $2^n - 2^{m+1}$ configurations $S_1^i(x)$ that spam the set of all first lines that respects the PBC. Let us examine the details with some illustrative examples.

Example 1: Consider a system size $L = 7$. This size can only be achieved with $n = 3$ and $m = 0$ (resulting in $L = 2^3 - 2^0 = 7$). Consequently, from Eq. (2.21) we find the basis element

$$\begin{array}{lll} S_1^1(x) = x + x^2 & S_1^2(x) = x^2 + x^3 & S_1^3(x) = x^3 + x^4 \\ S_1^4(x) = x^4 + x^5 & S_1^5(x) = x^5 + x^6 & S_1^6(x) = x^6 + x^7 \end{array}, \tag{A.1}$$

represented in Fig. 17. These configurations are "linearly independent" elements in the sense that it is impossible to construct any of them as a combination of the other five. One might wonder why $S_1^7(x)$ is excluded from (A.1), and the reason is that it is not an independent configuration, it can be constructed as

$$S_1^7(x) = x^7 + x = \sum_{i=1}^{6} S_1^i(x). \tag{A.2}$$

In fact, any other configuration that respects the periodicity can be constructed as combination of the $S_1^i(x)$ defined in (A.1). For example, the configurations

$$\begin{aligned} x + x^3 &= S_1^1 + S_1^2, \\ x + x^2 + x^4 + x^6 &= S_1^1 + S_1^4 + S_1^5, \\ x^2 + x^3 + x^4 + x^5 &= S_1^2 + S_1^4 \end{aligned} \tag{A.3}$$

are depicted in Fig. 18. Since the elements of (A.1) spam the space of configurations, for $L = 7$ the dimension of $\{S_1(x)\}$ is 6.

Configurations that cannot be constructed as combination of the elements of Eq. (A.1) do not form closed structures under PBC. For example, consider the configuration $\tilde{S}_1(x) = x + x^3 + x^4$, that cannot be construct combining the $S_1^i(x)$. This configuration do not satisfy $\tilde{S}_{1+7}(x) = \tilde{S}_1(x)$, instead

$$\begin{aligned} \tilde{S}_{1+7}(x) &= (1+x)^7 \, \tilde{S}_1(x) \\ &= \left(x^2 + x^3 + x^4 + x^5 + x^6\right)\left(x + x^3 + x^4\right) \\ &= x^2 + x^5 + {}^6 + x^7 \neq \tilde{S}_1(x), \end{aligned} \tag{A.4}$$

[1] These elements can be added and multiplied by a $\mathbb{Z}_2$ scalar α. The addition respect all axioms, including associativity and commutativity, which hold trivially. The identity element is $S_1^0 = 0$ (given by the "repetition code" $t_{1,i} = 0$ for all i)and each element is its own inverse. Scalar multiplication by $\alpha = 0$ or $\alpha = 1$ respect the axioms trivially.

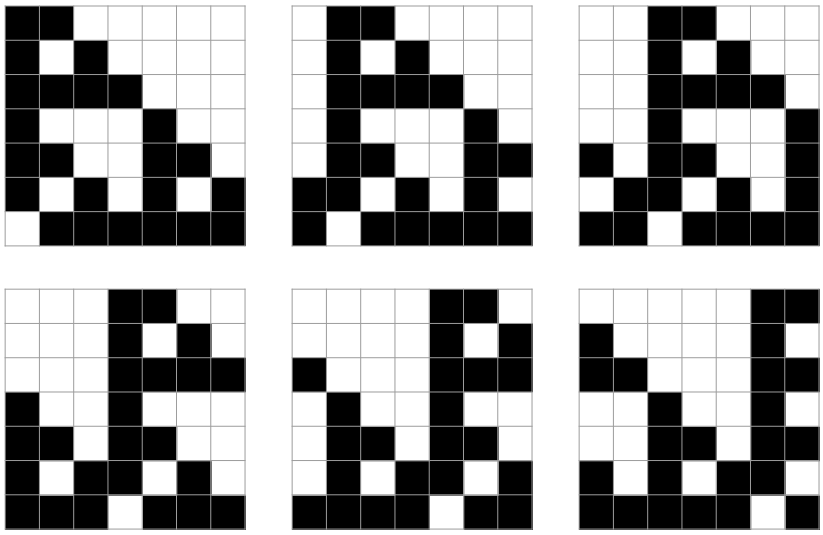

Figure 17 – The membranes generated by $S_1^i(x)$, where $i = 1, 2, \ldots, 6$, respectively, in system of size $L = 7$.

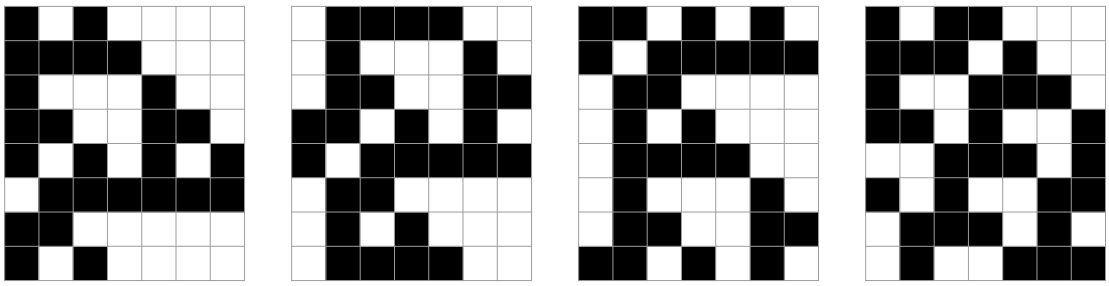

Figure 18 – The first three configurations are generated by the Eq. (A.3) and the last one by Eq. (A.4). The configurations are depicted with eight rows and seven columns, the extra row included in the end is equivalent to the first one by periodic boundary conditions. We can check that while the first three configurations are periodic in a size 7×7, the last one to not respects the periodicity.

as depicted in Fig. 18.

Example 2: Consider a system size $L = 6$. The basis for this size is defined Eq. (2.21) with $n = 3$ and $m = 1$. Consequently, the basis elements are

$$\begin{aligned} S_1^1(x) &= x + x^3 & S_1^2(x) &= x^2 + x^4 \\ S_1^3(x) &= x^3 + x^5 & S_1^4(x) &= x^4 + x^6, \end{aligned} \tag{A.5}$$

and they are represented in Fig. 19. Once again, none of this element can be constructed as combinations of the others. The other configurations that could appear as basis elements, $S_1^5(x)$ and $S_1^6(x)$, are excluded from Eq. (A.5) because they are linear combinations,

$$S_1^5(x) = x^5 + x = S_1^1(x) + S_1^3(x) \qquad \text{and} \qquad S_1^6(x) = x^6 + x^2 = S_1^2(x) + S_1^4(x). \tag{A.6}$$

Any other possible first-line configuration that can be constructed as combination (A.5),

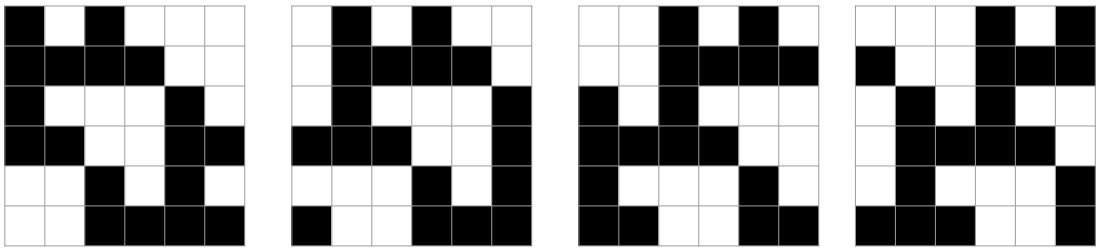

Figure 19 – The membranes generated by $S_1^i(x)$, where $i = 1$, 2, 3, and 4, respectively, in system of size $L = 6$.

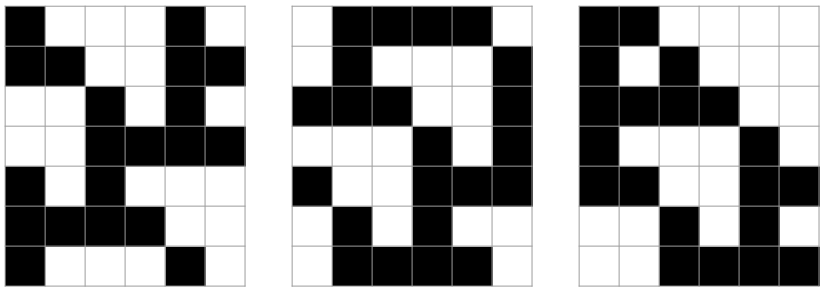

Figure 20 – The first and second configurations are generated by Eq. (A.7) and the last one is generated by Eq.(A.8). The configurations are depicted with seven rows and six columns, the extra row included in the end is equivalent to the first one by periodic boundary conditions. We can check that while the first two configurations are periodic in a size 6×6, the last one to not respects the periodicity.

such as

$$x + x^5 = S_1^1(x) + S_1^3 \qquad \text{and} \qquad x^2 + x^3 + x^4 + x^5 = S_1^2(x) + S_1^3(x), \tag{A.7}$$

are periodic, as depicted in Fig. 20

Configurations that cannot be expressed as combination of basis elements are excluded from the set of first lines because they do not form closed structures under PBC. For example, consider the configuration $\tilde{S}_1(x) = x + x^2$ that cannot be construct combining the $S_1^i(x)$ from Eq. (A.5). This configuration do not satisfy $\tilde{S}_7(x) = \tilde{S}_1(x)$, instead

$$\begin{aligned} \tilde{S}_{1+6}(x) &= (1+x)^6\, \tilde{S}_1(x) \\ &= \left(1 + x^2 + x^4 + x^6\right)\left(x + x^2\right) \\ &= x^3 + x^4 + ^5 + x^6 \neq \tilde{S}_1(x), \end{aligned} \tag{A.8}$$

as depicted in Fig. 20.

Example 3: For system sizes where $k \neq 1$, the first line is constructed with k copies of the $2^n - 2^m$ configuration, and it reflex on the degeneracy. Let us discuss an example to clarify this discussion. Consider $L = 9$, achieved only by $(k = 3, n = 2, m = 0)$. For this

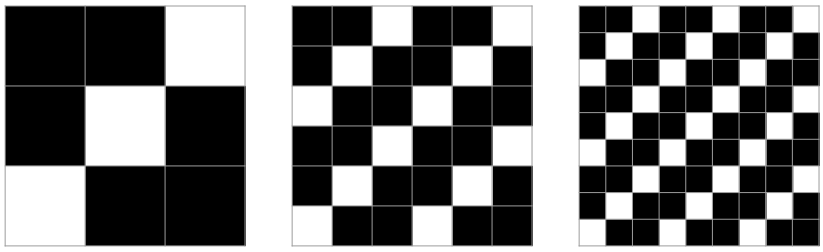

Figure 21 – Periodic configurations for 3×3, 6×6, and 9×9 respectively.

system size, the first line configuration, given by Eq. (2.21), is equivalent of 3 copies of the $S_1^i(x)$ of $L = 3$ as depicted in Fig. 21.

In a size 6×6 it is also possible to construct as copies of 3×3 configurations. However, the basis elements are given by the size 6 configuration, instead of two cpoies of size 3. Indeed, the 6×6 configuration depicted in Fig. 21 is generated by $S_1^2(x) + S_1^2(x) + S_1^3(x)$ from Eq. (A.5).